FINAL PUBLISHABLE REPORT

Grant Agreement number	18HLT06
Project short name	RaCHy
Project full title	Radiotherapy coupled with hyperthermia - adapting the biological equivalent dose concept

Project start date and duration:		01 June 2019, 42 Months
Coordinator: Giovanni Durando, INRIM Tel: +39 011 3919 353 E-mail: g.durando@inrim.it Project website address: https://rachy-project.eu		
Internal Funded Partners: 1. INRIM, Italy 2. NPL, United Kingdom 3. PTB, Germany 4. TUBITAK, Turkey 5. VSL, Netherlands	External Funded Partners: 6. ERASMUS MC, Netherlands 7. ICR, United Kingdom 8. ISS, Italy 9. OSR, Italy 10. TU Delft, Netherlands	Unfunded Partners: 11. VSPARTICLE, Netherlands
RMG1: INRIM, Italy (Employing organisation); VSL, Netherlands (Guestworking organisation)		

TABLE OF CONTENTS

1 Overview

The integration of radiotherapy with hyperthermia, which has been demonstrated to improve survival rate for patients with cancer, requires experimental studies to accurately assess the biological mechanisms involved at a cellular level. An increased understanding of the biological mechanisms involved will allow clinicians to prescribe the required thermal and radiation doses, according to an individual patient's needs. This project has developed and provided metrological support to achieve maximum synergistic advantage in the integration of radiotherapy (RT) oncology with different hyperthermia (HT) techniques, based on high intensity Therapeutic Ultrasound (TUS), Electromagnetic Radiation (EMR) and magnetic nanoparticles (MNPs) excited by AC magnetic fields. Heat delivery systems able to generate a uniform power deposition pattern in the target region with a closed-loop control which would maintain the defined temperature indefinitely have been developed and used for *in vitro* and *in vivo* tests. New systematic metrological approaches by using chemical metrology techniques such as FTIR spectroscopy as suitable non-invasive and non-ionising tissue diagnosis tools regarding chemical species combined with hyperspectral imaging (HSI) modalities at micrometre resolution have been used for the biomedical evaluations. The techniques and methods have been tested in preclinical cases and they are now available for clinical evaluation.

2 Need

Cancer is responsible for more than 1.3 million deaths in the European Union every year. With an ageing population, the incidence of cancer is rising. While cancer accounts for 22 % of all deaths for those over 65, this figure has grown to 38 % for people younger than 65, and it is the leading cause of premature death in 28 of the 53 regions in Europe. Even though current treatments available for cancer patients have improved, the survival of patients has not improved as desired, particularly for those diagnosed with advanced tumours.

The ability of hyperthermia to enhance the effects of radiotherapy has already been demonstrated, with results that include its ability to double the local control and survival rates. **Different heat delivery systems for hyperthermia treatments, TUS, EMR and MNPs excited by AC magnetic fields need to be designed, developed and characterised**.

In order to maximise treatment efficacy, it is mandatory to define the characteristics of the spatial and temporal temperature profiles required for the enhancement of radiotherapeutic effects, in terms of the relevant parameters to be monitored. It is necessary **to extend and improve quantification of the temperature exposure** obtained using hyperthermia techniques (TUS, EMR and MNPs), in combination with the energy deposited from radiotherapy, in *in vivo*, *in vitro* and *in silico* systems.

With regards to biological optimisation of exposure, the development of new innovative analytical tools for biological assessment using chemical metrology multimodal techniques such as vibrational spectroscopic techniques as suitable non-invasive and non-ionising tissue diagnosis tools, X-ray spectrometry traceable to the SI for elemental probing, and mass spectrometry combined with imaging modalities at nanometre resolution should be used for biological evaluations is needed. A metrological approach, related to the delivery and the evaluation of the combined therapy, is required to facilitate the **review of Relative Biological Effectiveness (RBE)** concept related to the radiotherapy combined with hyperthermia.

3 Objectives

The overall objective of the project is to develop measurement techniques and a metrological framework and that underpin the integration of clinical radiotherapy with hyperthermia treatments.

The specific objectives of the project are:

1. **To develop heat delivery systems for hyperthermia treatments (TUS, EMR and MNPs)** for use with radiotherapy. 2D and 3D measurement set-ups and validated modelling tools will be developed to estimate the spatial-temporal distribution of energy deposition.
2. **To extend and improve temperature exposure quantification** associated with the energy deposited from radiotherapy combined with hyperthermia methods (TUS, EMR and MNPs), in *in vivo* (37 °C to 50 °C), *in vitro and in silico* systems with a target uncertainty of < 10 %.
3. **To determine by *in vitro* and *in vivo* testing, using a metrological approach,** the efficiency of combined therapies: radiotherapy plus hyperthermia and reverse combination. The spatial-temporal

radiation-field characteristics are relevant for the combined radiotherapy/hyperthermia modalities, including radioactive magnetic nanoparticles for simultaneous radiation and heating.

4. **To develop innovative analytical tools for biological assessment** by using chemical metrology multimodal techniques as suitable non-invasive and non-ionising tissue diagnosis tools, and mass spectrometry combined with imaging modalities at nanometre resolution.
5. **To facilitate the review of Relative Biological Effectiveness (RBE) concept related to radiotherapy combined with hyperthermia.** The role of control parameters such as energy deposition in tissues, radiation dose and duration of the hyperthermia and/or radiation treatment will be taken into account.
6. **To facilitate the take up of the technology and measurement infrastructure developed in the project** by the measurement supply chain (accredited laboratories, instrumentation manufacturers), standard developing organisations (IEC, ISO) and end users (e.g., hospitals and health centres). This should include a close interaction with clinicians to assess the applicability of the combined therapy for future trials on patients.

4 Results

4.1 Heat delivery systems for hyperthermia treatments (TUS, EMR and MNPs) for use with radiotherapy

Rationale: The purpose of this objective was to develop heat delivery systems for hyperthermia treatments (TUS, EMR and MNPs) for use with radiotherapy. 2D and 3D measurement set-ups and validated modelling tools will be developed to estimate the spatial-temporal distribution of energy deposition.

New experimental and modelling methodologies were developed to enable the prediction of power deposition, temperature levels and profiles within tissue-mimicking materials and biological media during TUS, EMR and MNP-based hyperthermia. The temperature profile will be measured during exposure, to ensure a safe and effective treatment, Figure 1.

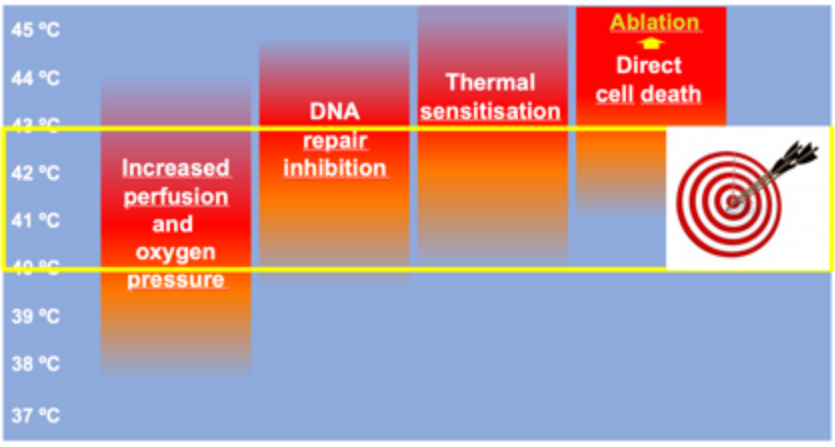

Figure 1, Biological mechanisms of hyperthermia

4.1.1 Hyperthermia mediated by TUS

Far Field Method, FFM: A system based on HIFU transducers using their far field properties was developed by INRIM, Figure 2.

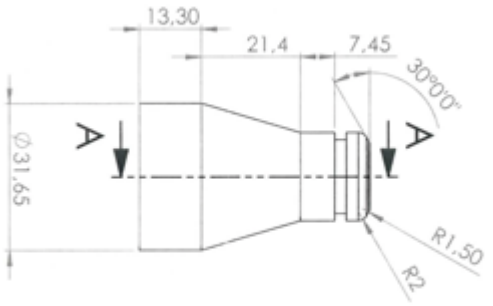

Figure 2 INRIM transducer comprising a SU103 S/N 101, Sonic Concepts transducer with stand-off cone which was filled with deionized, degassed water, and fitted with a Mylar acoustic window for measurements.

The HIFU transducer, (SU103 S/N 101, Sonic Concepts). The center frequency of the transducer was 3.57 MHz. was focused (diameter 23 mm, radius of curvature 35 mm) and a stand-off cone (height 49.50 mm) was attached to the face, Figure 2. The cone could be replaced with others of different dimensions designed for specific exposure areas. The adjusted transducer was characterized in terms of field mapping, acoustic pressure output and acoustic power output using NPL's calibration scanning tank and secondary standard power calibration service., Figure 3.

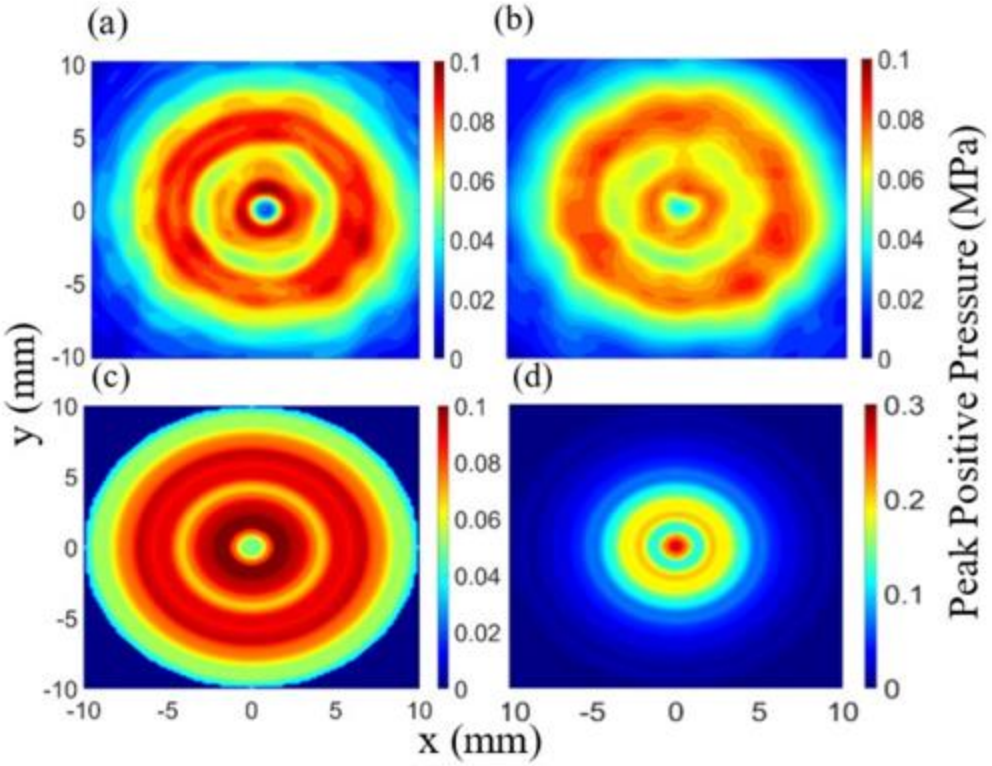

Figure 3 The xy plane field map (a) without the stand-off cone and (b) with the stand-off cone measured at 30 mm in the far field and approximated fields at (c) 30 mm, for comparison, and (d) 15 mm after the focus, where exposures were performed.

With this insonation system it was possible to treat tumour tissue up to 10 mm diameter with hyperthermia, without using the motorized positioning translator coupled to the HIFU transducer. The designed system has been used for assessing the potential of radiotherapy combined with hyperthermia in initial phantoms and preclinical small animal studies.

Acoustic Hologram Lenses, AHL: Holograms allow a simultaneous targeting providing a uniform thermal dose. Ultrasound hyperthermia delivery systems based on acoustic hologram lenses that produce a more uniform thermal dose over complex in vitro and in vivo biological targets than a single geometric focus HIFU transducer have been developed by ICR and Guy's St Thomas' Hospital (Project Stakeholder Committee). The *in vitro* set up was designed for simultaneous treatment of 3D cell aggregates (spheroids) using an absorbing phantom with multiple wells, each holding a tumour spheroid, Figure 4.

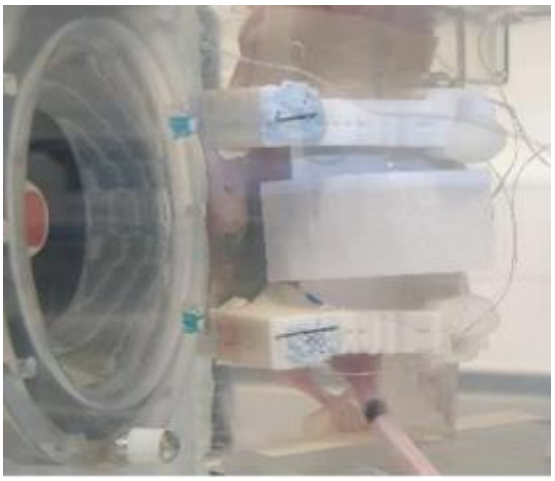

Figure 4 Ultrasound imaging guided therapy ultrasound system with 9-foci transparent lens used for in vivo delivery of hyperthermia to U87 subcutaneous tumours.

The acoustic field produced by the holographic lenses designed for spheroid exposures was measured using a hydrophone in a water tank filled with degassed, deionized water at room temperature. The hydrophone was mounted on an automated 3D positioning system. The 1.66-MHz source is a H148-MR Sonic Concepts piezo-ceramic transducer, with a 63.2-mm radius of curvature, 64-mm outer diameter and 23-mm inner hole diameter, mounted in a fixed position and driven with sinusoidal pulsed-burst signals from a signal generator after being amplified. Signals were recorded using a digital oscilloscope taking a time window of 20 µs when arising steady state, to avoid the transitional period, Figure 5. The *in vitro* set up was designed for simultaneous treatment of 3D cell aggregates (spheroids) using an absorbing phantom with multiple wells, each holding a tumour spheroid.

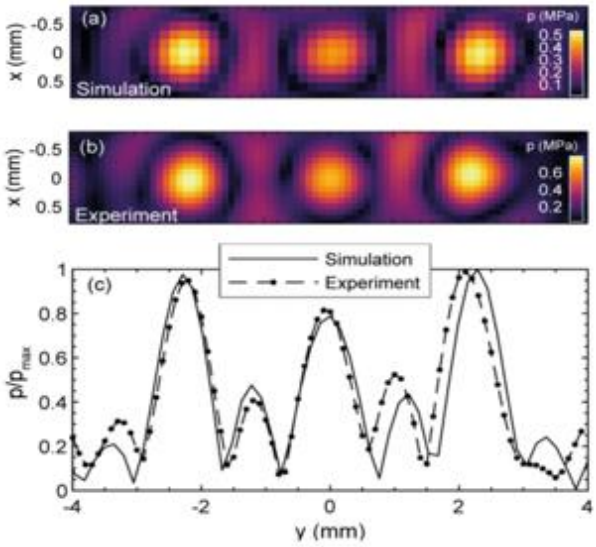

Figure 5 (a) Acoustic simulation at z = 40 mm (lens central acoustic maximum) for the three-foci lens. (b) Corresponding acoustic measurement. (c) Normalized linear plot of the measured and simulated acoustic fields through the central focal peak.

4.1.2 Hyperthermia mediated by EMR

INRIM, ERASMUS MC and TU Delft have developed a radiofrequency (RF) electromagnetic applicator operating at 434 MHz, specifically engineered for in vitro tests on 3D cell cultures. The applicator has been

designed with the aid of an extensive modelling analysis, which combines electromagnetic and thermal simulations. The heating performance of the built prototype has been validated by means of temperature measurements carried out on tissue-mimicking phantoms and aimed at monitoring both spatial and temporal temperature variations. To support the design of the RF applicator, in terms of optimal dimensions, power deposition and heating efficiency, INRIM performed EM simulations followed by heat transfer modelling. Both types of simulations were carried out by means of the advanced computation platform Sim4Life (v6.2, ZMT, Zurich, Switzerland). A non-uniform grid was used to discretize the 3D domain under study Ω, which is a rectangular prism including the whole volume of the applicator, and expanded by 17.3 cm in each direction, so that its boundary ∂Ω does not influence the electric field generated by the applicator. Table 1 shows Electrical and thermal properties of the materials considered in the simulations.

Table 1

Material	ρ [kg/m^3]	σ [S/m]	ε_r [1]	C_p [J/(kg·K)]	k [W/(m·K)]
HDPE [1]	950	0.00001	2.1	1900	0.5
PVC [1]	1380	0.0001	3	1250	0.2
Agar gel	1000	0.755	74	4181	0.563

[1] ε_r stands for relative permittivity, HDPE for high-density polyethylene and PVC for polyvinyl chloride.

The RF applicator is designed according to the TEM mode in a coaxial cable, rescaling the system proposed in to obtain an applicator suitable for in vitro tests and, potentially, for preclinical tests on small animals. The RF applicator based on a coaxial TEM system with well-focused heating is able to generate a uniform power deposition pattern and a controlled temperature rise in a 1 cm^3 target region size, at a frequency of 434 MHz. As schematized in Figure 6, this consists in an outer cylindrical conductor (in red) connected to the metallic shield of the feeding coaxial cable and a hollow inner cylindrical conductor (in blue), connected to the coaxial cable target region, centered in the aperture, where the phantom (in green) is positioned after centered in the aperture, where the phantom (in green) is positioned after being inserted i in a PVC tube (in yellow).

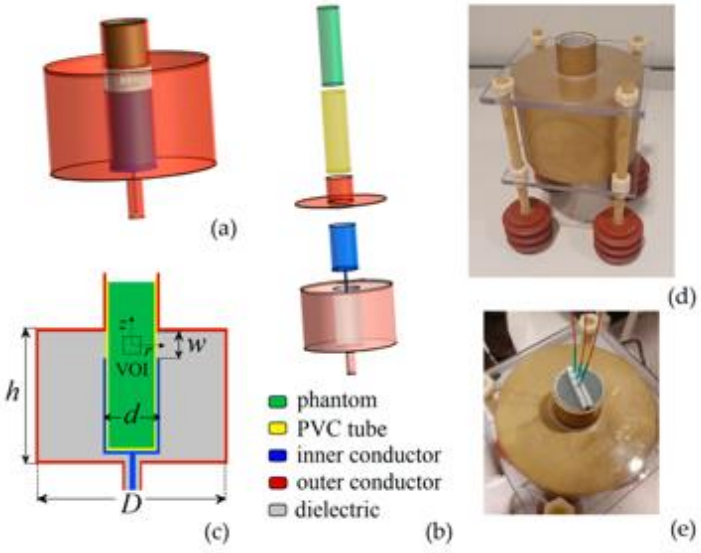

Figure 6 Schematics of the RF applicator:(a) 3D view with mounted components; (b) main components with representation of insertion; (c) longitudinal cross-section with indication of the main parameters, i.e., d is the outer diameter of the inner conductor, D is the inner diameter of the parameters of the outer conductor, w is the aperture width and h is the external height of the outer conductor. The dashed line indicates the target region or volume of interest (VOI). Pictures of the RF applicator: (d) dashed line indicates the target region or volume of interest (VOI). Pictures of the RF applicator: frontal view, with insulating and mechanical support; (e) top view showing the phantom with the (d) frontal view, with insulating and mechanical support; (e) top view showing the phantom with the fiber-optic thermometers.

Within the aperture, the EM field is a PVC tube (in yellow). Within the aperture, the EM field is circumferential and radiative, circumferential and radiative, with an expected heating focus in correspondence of the with an expected heating focus in correspondence of the aperture center. The space between aperture center. The

space between the two conductors is filled with a dielectric medium the two conductors is filled with a dielectric medium (in light grey), made of HDPE (in light grey), made of HDPE.

INRIM in collaboration with ERASMUS MC have performed the parametric analysis for the design of the RF applicator. The shape and size of the final prototype derives from the following requirements:

- the aperture has to be properly dimensioned to guarantee the accommodation of standard vials for in vitro tests on 3D cell cultures;
- the heating focus has to be positioned within a cubic target region of 1 cm3 volume (VOI), where a homogeneous power deposition should be obtained
- under operating conditions, the applicator should match as close as possible a load with an impedance Z of 50 Ω, in order to minimize reflections and avoid the need of a matching network for its operation.

As an example, Figure 7 reports the spatial distribution of the specific adsorption rate (SAR) over a longitudinal cross-section of the RF applicator, for w = 1.7 cm, d = 3.5 cm and D = 11.7 cm.

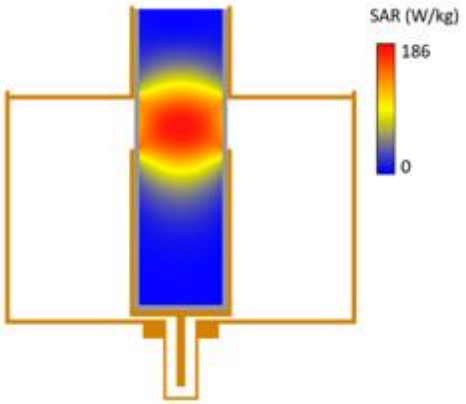

Figure 7 Spatial distribution of the specific adsorption rate (SAR) in the phantom, calculated over a longitudinal cross-section of the RF applicator

4.1.3 Hyperthermia mediated by MNPs

The hyperthermia efficacy of MNPs is usually measured by means of the specific loss power (SLP), also known as specific absorption rate (SAR), which expresses the power dissipated per unit mass of magnetic material. The mechanisms contributing to SLP involve the alignment of the MNP magnetic moment along the direction of the AC magnetic field by the rotation of the magnetization vectors within MNPs or by the mechanical rotation of the MNPs in the medium (Brownian relaxation).

Three types of magnetic nanomaterials for magnetic hyperthermia application, namely Fe3O4 nanoparticles, Fe70Pd30 nanodisks and hybrid 103Pd-FeO nanoparticles were designed and prepared:

- Fe3O4 nanoparticles, were synthetized by INRIM and TUBITAK, with diameters variable in the range 10-200nm, calorimetric measurements have been performed for selection of the batches more efficient for magnetic hyperthermia, i.e. the largest size ones, which contribute to the heating with hysteresis losses.
- Fe70Pd30 nanodisks, were prepared by INRIM and TUBITAK, by means of self-assembling nanosphere lithography. The three sets of nanodisks were characterised in terms of size (scanning electron microscopy) and static magnetic properties (vibrating sample magnetometry).
- Non-radioactive 103Pd-FeO nanoparticles (Pd core and FeO shell), were prepared by TU Delft (in collaboration with VSPARTICLE), VSL and ERASMUS MC, with both spark-ablation and wet-chemistry methods; the latter seems to be more advantageous in terms of effective particle's size and yield that could be achieved.

The presence of many influencing parameters (material features, size, shape, aggregation state) makes it complex to distinguish and quantify their contribution to the heating performance, requiring before in vitro and in vivo tests an exhaustive experimental and modelling analysis of MNP magnetic and calorimetric properties.

The best heating efficacy was found using of Fe3O4 nanocubes. INRIM with support of TUBITAK and TU Delft performed detailed characterization of Fe3O4 MNPs with cubic shape, produced via hydrothermal route by

varying synthesis parameters (temperature and reaction time). Four samples were prepared, Figure 8, with average size between 15 nm and 160 nm, and magnetic behaviour that mainly falls in the single domain ferromagnetic regime or in the multi-domain one, as demonstrated by magnetometric measurements combined with micromagnetic calculations of the static hysteresis loops with size around 20 nm.

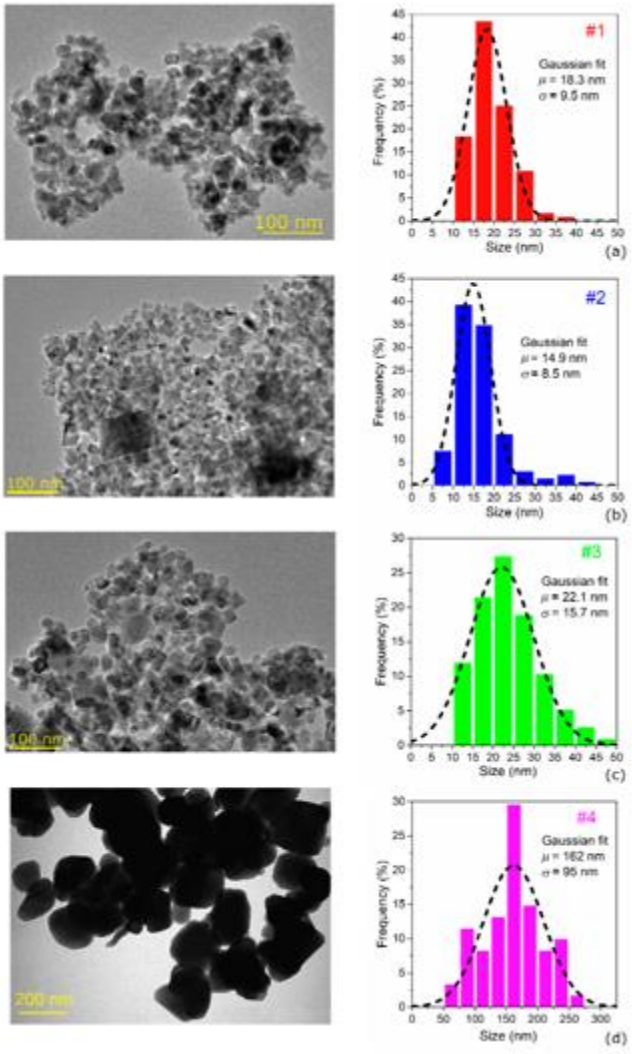

Figure 8 Transmission Electron Microscopy (TEM) images of the four samples of Fe3O4 MNPs, with relative size histograms fitted by a Gaussian function having mean value μ and standard deviation σ.

The mean size is equal to: (a) 18.3 nm for sample #1; (b) 14.9 nm for sample #2; (c) 22.1 nm for sample #3; (d) 162 nm for sample #4.

Fe3O4 NPs were formed during the following chemical reaction:

$$Fe^{2+}+2Fe^{3+}+8OH^{-} \rightarrow Fe_3O_4+4H_2O \quad (1)$$

To support the experimental magnetic characterization, INRIM in collaboration with TUBITAK calculated the hysteresis loops of the Fe3O4 MNPs by using the 3D micromagnetic code, developed by INRIM, which solves the Landau–Lifshitz–Gilbert (LLG) equation. According to TEM analysis in the simulations, the MNPs were approximated as truncated cubes with sizes ranging from 20 nm to 200 nm (between 10 nm and 20 nm transition from superparamagnetism to ferromagnetism is expected). Rounded corners were introduced, modelling the MNPs as objects obtained by intersecting a cube of side l with a sphere of diameter d. Figure 9.

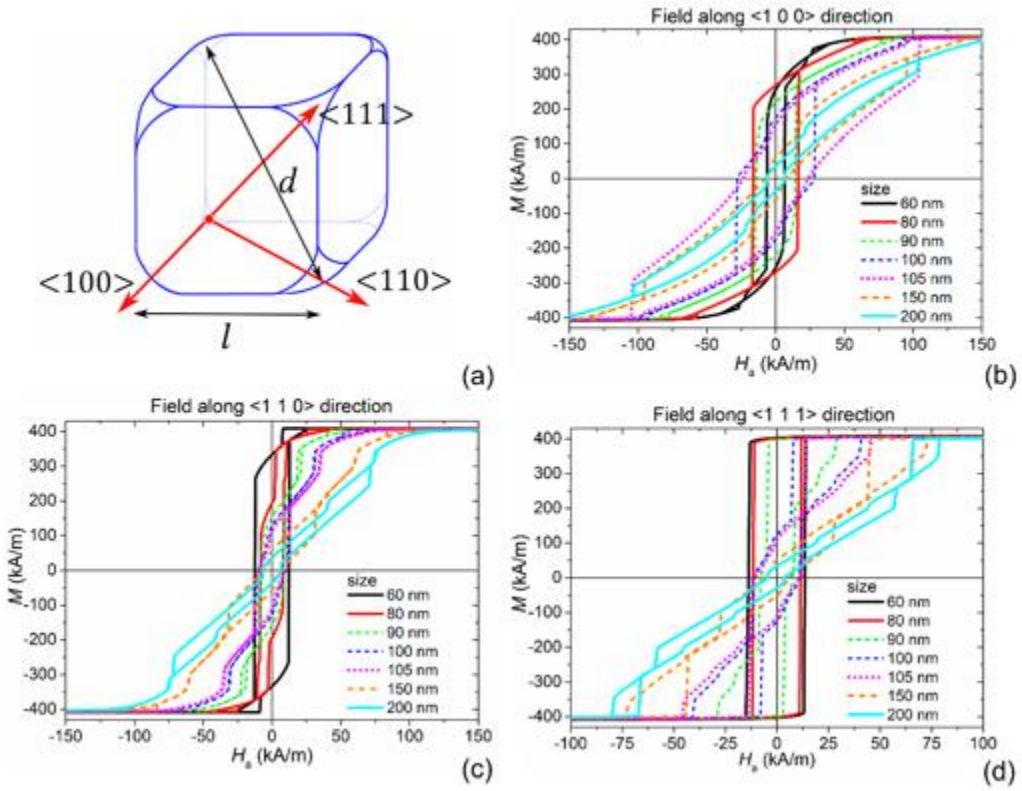

Figure 9 (a) Schematic of the cubic Fe3O4 MNP with size *l*; the red arrows identify the three magnetocrystalline anisotropy axes, parallel to cube edge (<100> direction), cube face diagonal (<110> direction) and cube diagonal (<111> direction). Static hysteresis loops for a single Fe3O4 nanocube with l ranging from 60 nm to 200 nm, calculated by applying the magnetic field along (b) <100>, (c) <110> and (d) <111> directions.

When 20 ≤ *l* < 80 nm, small variations were found in the loop shape and size. In particular, a single-domain behavior was observed, with the effective hard axis along the cube edge or <100> direction (Figure 9b) and an effective easy axis along the cube diagonal or <111> direction (Figure 9d), due to the dominance of magnetocrystalline anisotropy effects.

Conclusion:

New experimental and modelling methodologies were developed to enable the prediction of power deposition and temperature profiles within tissue-mimicking materials and biological media during TUS, EMR and MNP-based hyperthermia.

A system based on HIFU transducers (Sonic Concepts SU-103) using their far field properties was developed. With this approach it is possible to treat tumour tissue up to 10 mm diameter with hyperthermia, without using the motorized positioning translator coupled to the HIFU transducer. The system was tested in vivo by measuring the temperature induced by US fields. Ultrasound hyperthermia delivery systems based on acoustic hologram lenses that produce a more uniform thermal dose over complex in vitro and in vivo biological targets than a single geometric focus HIFU transducer have been developed. The *in vitro* set up was designed for simultaneous treatment of 3D cell aggregates (spheroids) using an absorbing phantom with multiple wells, each holding a tumour spheroid.

An RF applicator based on a coaxial TEM system with well-focused heating was designed and fabricated for EMR hyperthermia. This system is able to generate a uniform power deposition pattern and a controlled temperature rise in a 1 cm^3 target region size, at a frequency of 434 MHz and has been shown to be suitable for use as a calibrated setup for hyperthermia tests on tissue-mimicking materials, 3D cell cultures and tumour organoids.

Magnetic hyperthermia experiments were conducted in a custom-built laboratory setup on a set of samples, comprising Fe_3O_4 nanoparticles and $Fe_{70}Pd_{30}$ nanodisks suspended in liquid. The heating properties were determined by the magnetic single- or multi-domain configuration and by the competition between magnetocrystalline and shape anisotropies. The results demonstrated that a larger concentration of MNPs in phantoms is needed to obtain a temperature rise than in liquid.

4.2 To extend and better quantify temperature exposure evaluation

Rationale: The purpose of this objective was to extend and improve temperature exposure quantification associated with the energy deposited from radiotherapy combined with hyperthermia methods (TUS, EMR and MNPs), in in vivo (37 °C to 50 °C), in vitro and in silico systems with a target uncertainty of < 10 %.

4.2.1 Temperature exposure quantification due hyperthermia mediated by TUS

Far Field Method, FFM:

The heating efficiency of the insonation system, described in 4.1.1, is characterized by performing two types of thermometric measurements conducted by NPL in collaboration with PTB and TUBITAK. The ultrasound transducer used for this work was HIFU device, SU103. A stand-off cone, designed and produced by INRIM, was attached and filled with degassed deionized water (conductivity < 5μS·cm-1) and sealed with a 12 μm thick Mylar layer. Prior to the system being switched on, a specifically designed phantom was submerged in a water bath and the stand-off cone at the face of the transducer was positioned in contact with the in house manufactured phantom. The phantom, developed by NPL, was designed with the following criteria: to simulate biological tissue acoustically and thermally, to provide real-time feedback of the temperature and to include a thermochromic material to provide both an indicator of exposure area and the temperature reached in a biologically relevant environment. The phantom was designed containing fine wire thermocouples across the surface (Figure 2) held in place in a 3D printed holder. There were 5 K-type 75 μm diameter thermocouples (5SRTC-TT-KI-40-1M, Omega, UK) placed across the phantom (1) at the centre (2) at 2.5 mm from the centre, (3) at 5 mm, (4) at 7.5 mm and (5) at the reference point (12.5 mm), Figure 10

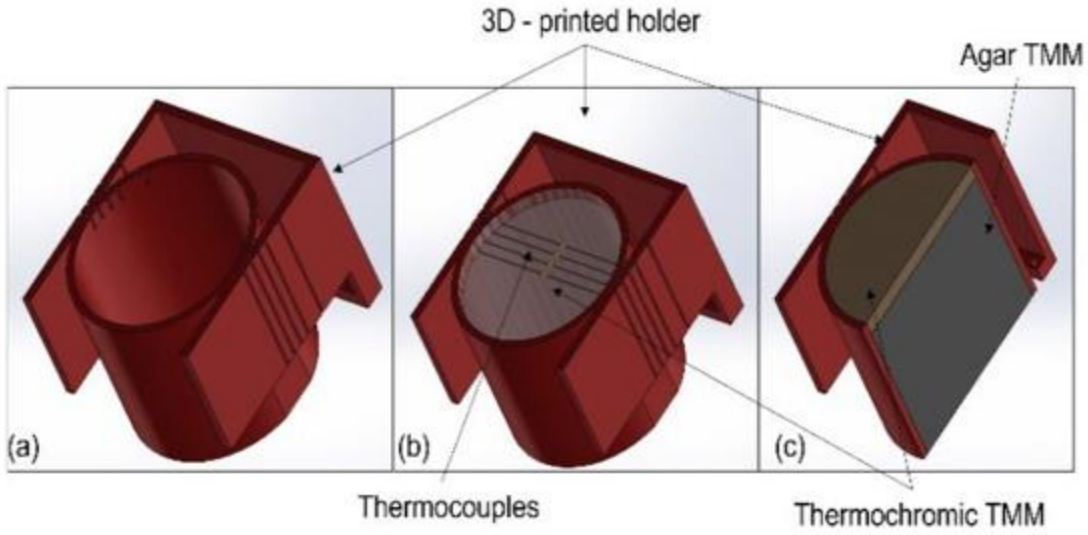

Figure 10 The designed phantom test device (a) the 3D printed holder, (b) with transparency of the thermochromic layer to show thermocouple positions and (c) a cross section showing the TMM layers. The overall phantom assembly was 35 mm in depth and 44 mm in diameter, the agar TMM section had a height of 32 mm and the thermochromic layer 3 mm, both had a diameter of 38 mm.

The water bath was heated to 37°C and the system switched on. The target temperature was set within the MATLAB code: the target here was set to body temperature, 37 °C, plus 6 °C: 43°C, and the upper and lower limits around this temperature set as T_{high} and T_{low}, respectively. When the temperature was read across the 5 thermocouples, the highest thermocouple temperature was compared to these values, if the temperature was lower than T_{low} the voltage to the transducer was increased by 5 mV_{pp}, if the temperature was above T_{high}, the voltage to the transducer was decreased by 5 mV_{pp}. The temperature was queried every 5 seconds for 4 minutes to first achieve heating in the target region and then maintain the temperature within this range. Thermocouple voltages and temperatures were recorded at each time point. After 4 minutes the transducer was switched off, and the phantom began to cool, the temperature was similarly queried and recorded every 5 seconds for 4 minutes in this period to determine the cooling curve, typical temperature measurements

The hyperthermia delivery system was found to provide control of exposure based on the set temperature limits throughout all ten exposures. An example of the results is shown in Figure 11.

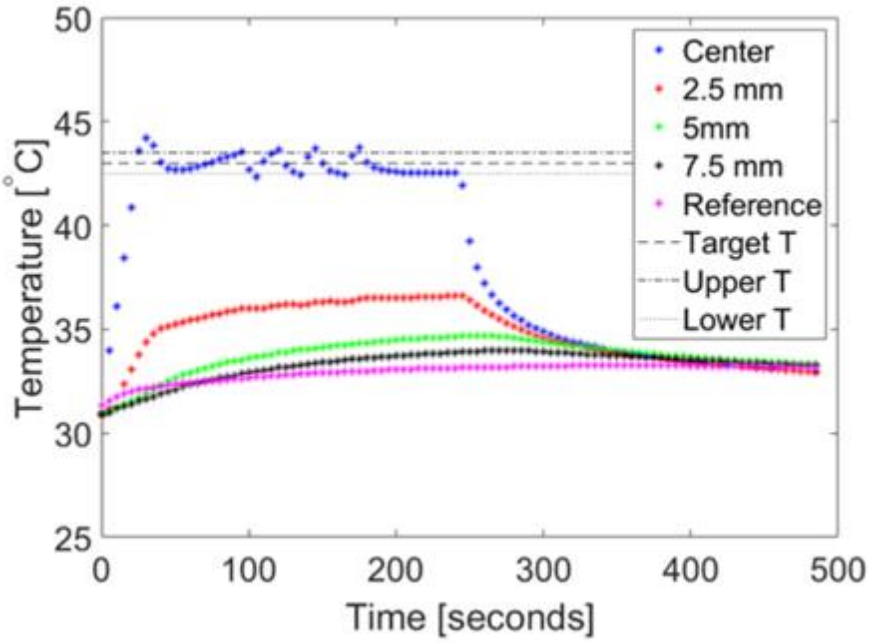

Figure 11 Example of the recorded thermocouple temperatures and applied voltages from the phantom exposures, from run 10 (a) temperature versus time, where the upper limit on temperature was 43.5 °C and the lower limit 42.5 °C

The system was tested on a newly designed custom-built phantom with controlled thermal properties and containing embedded thermocouples. Additionally, a layer of thermochromic material was fixed above the thermocouples and the recorded temperature increase was compared to the RGB (red, green, and blue) color-change in the material. The thermochromic layers from the phantom after exposure were compared to samples heated in a water bath to various fixed temperatures, Figure 12 illustrates these results. TMM samples in tubes were heated in a water bath to various temperatures between 25°C and 60°C.

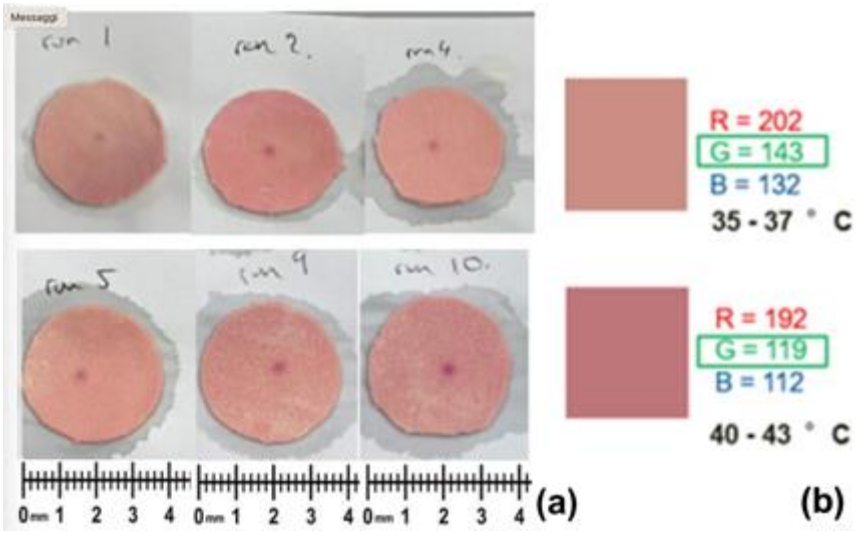

Figure 12 (a) Various examples of the thermochromic TMM layers after exposure, showing a confined area of darker lesion (b) Examples of the analysis on areas in the exposure region and outside the exposure region, indicating that the temperature achieved was at the target temperature and that the region exterior to this remained at body temperature.

Each of the single use thermochromic TMM layers after exposure showed a confined area of darker lesion where the exposure occurred, and no other lesions were present. This area matched the field maps for this position (15 mm), Figure 13.

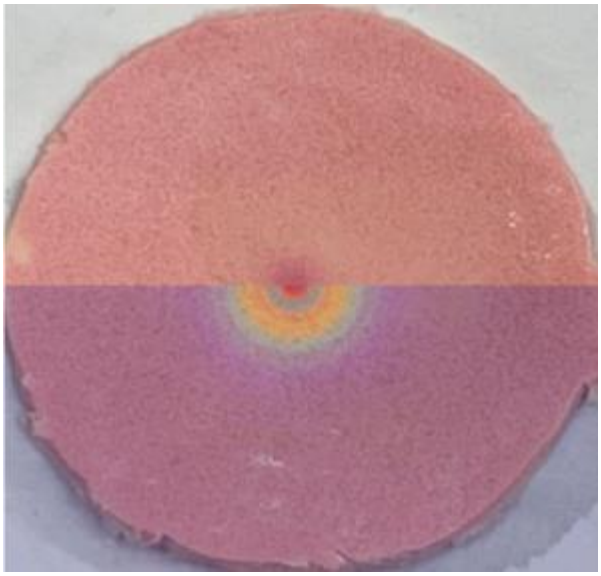

Figure 13 Overlay of the semi-transparent half-field map at 15 mm, where the exposures were performed on a sample of the thermochromic TMM, showing the region of exposure was well matched.

An ultrasound numerical tool, based on the Westervelt equation, for the simulation of the ultrasound propagation in heterogeneous media like fluids or tissues and the calculation of power deposition was developed by ISS, INRIM and NPL. The results were compared with two commercial solvers based on the Angular Spectrum Method and the commercial k-wave code. All these results were compared with hydrophone measurements for pressure and thermocouple measurements for temperature increase. All tests show a very high consistency in pressure results, with differences below 1% and consistent results in temperature measurements, with agreement down to 8%, with the expected overestimation of sensor measurements due to viscous heating.

Acoustic Hologram Lenses, AHL

The heating efficiency of the Acoustic Hologram Lenses, AHL, described in 4.1.1, is characterized by performing thermal measurements conducted by ICR in collaboration with Guy's St Thomas' Hospital.

Both, *in vitro* and *in vivo* ultrasound hyperthermia systems, developed by ICR and NPL, consist of a focused ultrasound transducer coupled to a holographically-designed, 3D-printed acoustic lens. The *in vitro* system used for spheroid exposures uses a 63.2-mm radius of curvature, 64-mm outer diameter and 23-mm inner hole diameter focused ultrasound transducer with 1.66-MHz central frequency, while the *in vivo* system transducer had physical dimensions of 50 mm radius of curvature, 65 mm outer diameter and 40 mm inner hole diameter, with 1.5-MHz central frequency. To both evaluate the thermal profile produced with the holographic lenses and to expose (500 to 800 micron diameter) spheroids to a precisely controlled thermal dose, a new exposure system was designed. The system needed to absorb ultrasound and create heating (of spheroids) and be instrumented so that temperature (thermal dose) could be accurately monitored.

In order that multiple spheroids could be exposed to the same thermal dose simultaneously, it holds three spheroids in separate miniature wells (0.7 mm deep and 1 mm diameter) spaced 2 mm apart, as shown in Figure 14 (b). Thermocouples (detailed below) were manually placed in the gel mould so they would be embedded in the middle of each well but 0.5 mm below the bottom of it to provide an estimate of the temperature that each well/spheroid experiences, see Figure 14.

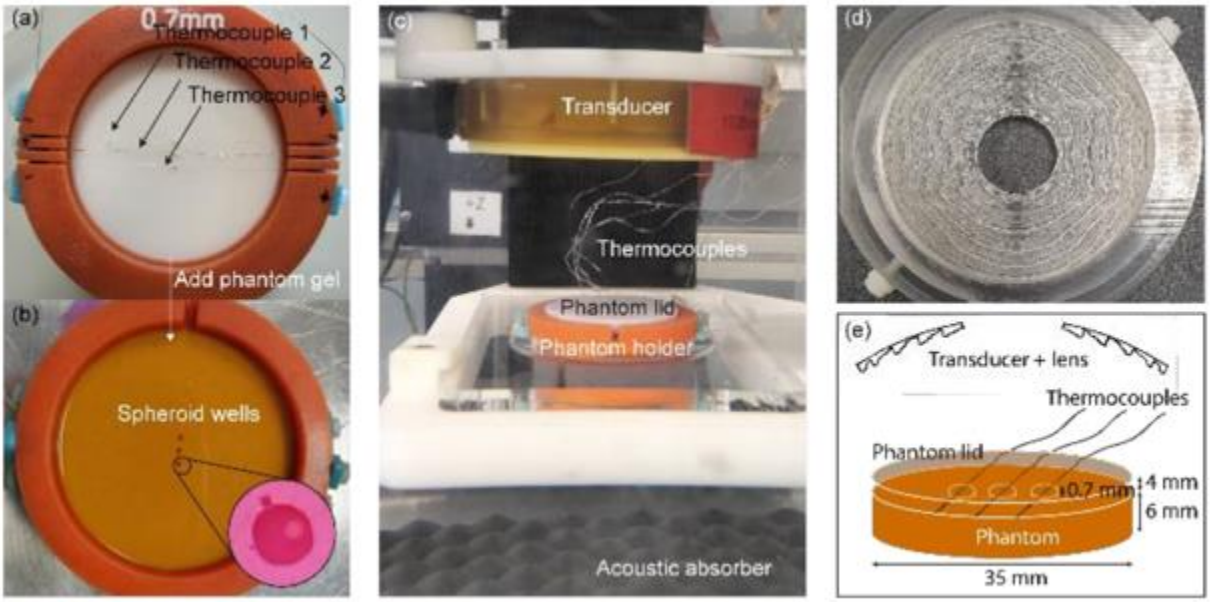

Figure 14 The holographically designed lens, high intensity focused ultrasound transducer and absorbing gel spheroid holder used in hyperthermia experiments. The mould (a) used to form the absorbing gel phantom (b), with 3 miniature wells in which a spheroid could be placed. The arrangement used to exposure the spheroids to ultrasound (c). The 3D-printed lens with the holder to be mounted on top of the transducer. (d). Schematic showing the thermocouples which are embedded in the absorbing gel at the base of each miniature wells.

Each thermocouple in the phantom holder was localised using the transducers geometric focus. Their positions, relative to the central one, were (0, -2,0) ± 0.25mm and (0, 2,0) ± 0.25mm. Using the 3-foci holographic lens and continuous exposures at 85 mV_{pp}, sonications were performed moving the transducer from -1 mm to 1 mm around the central location, with spatial steps of 0.25 mm and exposure times of around 5 minutes, thermal profiles recorded at each transducer position for all three thermocouples are shown in Fig. 15.

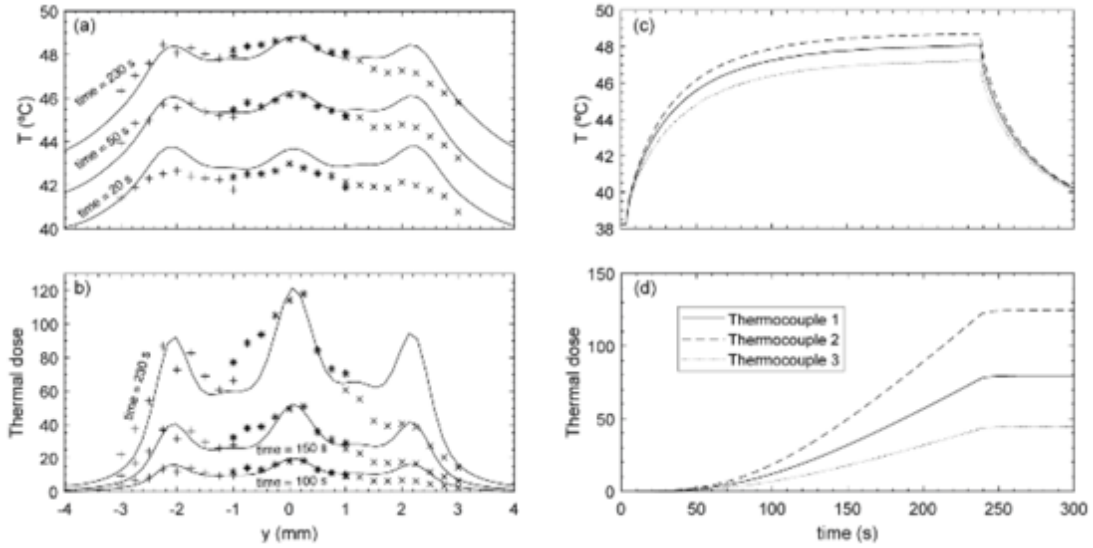

Figure 15 Temperature profile at different time instants in simulation (solid line) and measured experimentally with each thermocouple (**+** symbol for thermocouple 1, ***** symbol for thermocouple 2 and **×** symbol for thermocouple 3). (b) Thermal dose profile at different time instants in simulation (solid line) and measured experimentally with each thermocouple (**+** symbol for thermocouple 1, ***** symbol for thermocouple 2 and **×** symbol for thermocouple 3). (c) Experimental temperature profile at the central position measured by each thermocouple. (d) Experimental thermal dose profile at the central position measured by each thermocouple.

4.2.2 Temperature exposure quantification due hyperthermia mediated by EMR

The heating efficiency of the built RF applicator, described in 4.1.2, was characterized by performing two types of thermometric measurements conducted by INRIM. One aims at characterizing the temporal response of the system as a function of the effectively supplied power, monitoring the heating and cooling transients in a set of points within the phantom. The second one is finalized to the characterization of the heating focus, through the measurement of the temperature spatial distribution at the end of the heating transient.

To this aim, INRIM monitor the temperature along time with three fiber-optic sensors, placed at 0.5 cm intervals along the radial direction, i.e., at zero, 0.5 cm and 1 cm distance from the central axis of the cylindrical phantom as shown in Figure 16 a.

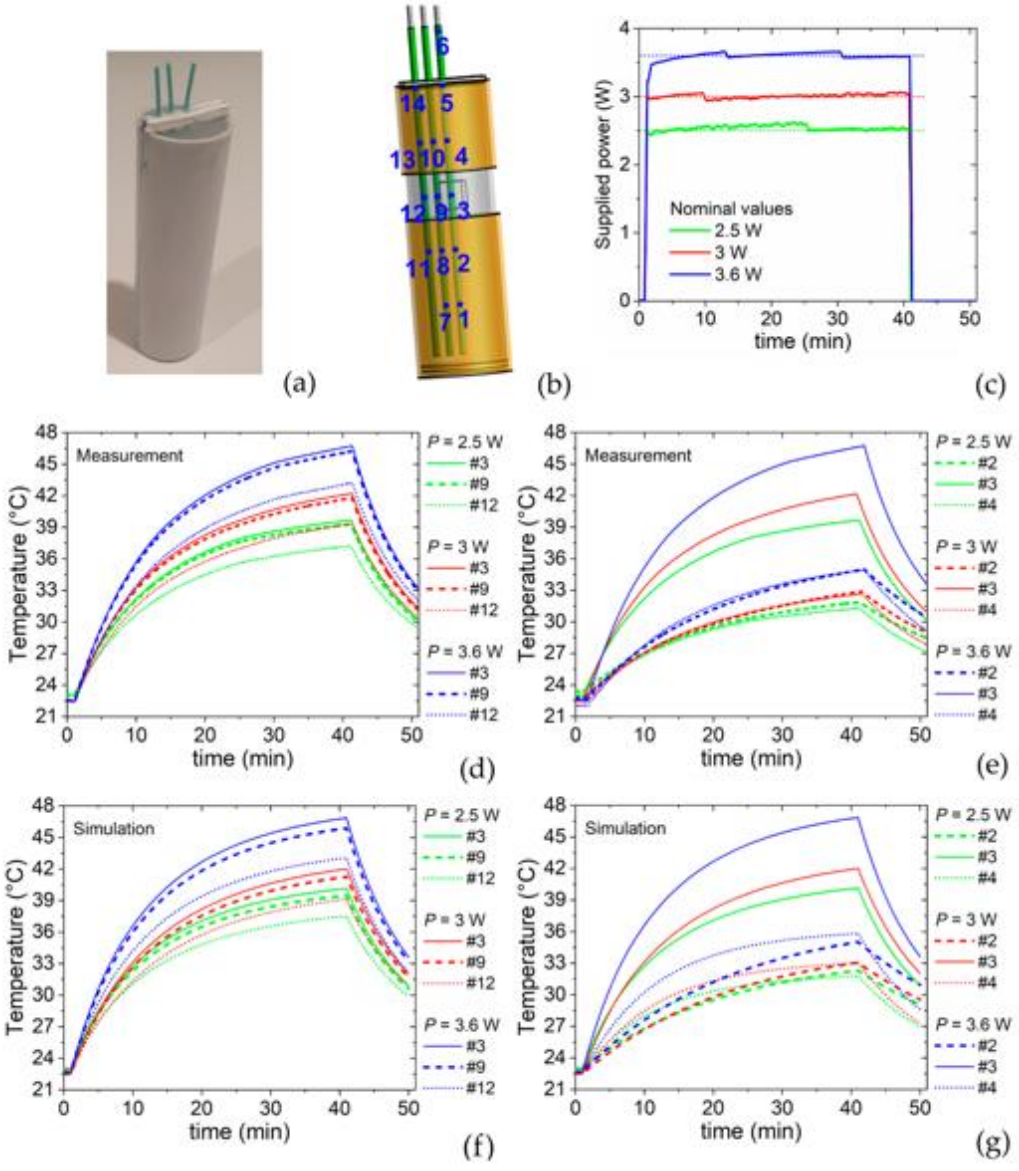

Figure 16 (a) Picture of the phantom with the three fiber-optic thermometers arranged along the radial direction. (b) Schematics of the phantom, showing the position of the VOI and of the 14 measurement points distributed along the fiber-optic thermometers. (c) Time evolution of the effectively supplied power for three power nominal values (2.5 W, 3 W and 3.6 W, as indicated by dashed lines). Heating cooling transients as a function of supplied power levels: measured time-evolution in points (d) #3, #9 and #12, and (e) #2, #3 and #4; simulated time-evolution in points (f) #3, #9 and #12, and (g) #2, #3 and #4.

Each fiber-optic sensor, which has multiple measuring points along its length with adjacent distance of 2 cm, is inserted in the phantom, so that one of the measuring points (the one numbered as #3) is positioned in correspondence of the VOI center (see the schematic in Figure 16 b).

As a target temperature in the VOI centre, the consortium chose 43°C. For the determination of the required power levels, the experiments are conducted by supplying the applicator for 40 min, while keeping the effectively supplied power (input power minus reflected power) as close as possible to the nominal values of 2.5 W, 3 W and 3.6 W (Figure 16 c). Figure 16 d reports the time evolution of the temperature recorded at the measurement points #3, #9 and #12, which are distributed along the radial axis with origin in the VOI centre. The maximum temperature, measured in point #3, is equal to 39.7 ◦C, 42.2 ◦C and 46.7 ◦C for the power levels of 2.5 W, 3 W and 3.6 W ◦C, respectively. As demonstrated by the comparison of Figure 16 d, Figure f, a very similar behaviour of measured and simulated thermal curves is indeed found for the entire time interval in measuring points #3, #9 and #12. However, along the vertical axis, the simulated thermal curves show slight differences from the measured ones, especially during the heating transient; the measured and simulated peak temperatures differ less than 0.5 ◦C (comparison of Figure 16 e, Figure g).

4.2.3 Temperature exposure quantification due hyperthermia mediated by MNPs

Thermometric measurements of the Fe3O4 MNPs, described in 4.1.3, were performed by INRIM in collaboration with TUBITAK.

A fiber optic thermometer records the temperature increase in the magnetic solution induced by the power released by the MNPs and the subsequent cooling to room temperature after the magnetic field is turned off. The experimental curves were analysed by an ad hoc thermodynamic analytical model, in order to obtain a direct estimation of the SLP values. This model takes into account the parasitic heating of the water and the heat exchange with the surrounding environment under non-adiabatic conditions, which can be limited by inserting the sample within a thermal insulating polystyrene foam tube.

Figure 17 shows the time evolution of the temperature of the magnetic solution, measured for samples #3 and #4 under the application of an AC magnetic field with a frequency *f* of 100 kHz and a peak amplitude in the range 24–48 kA/m was applied to an aqueous suspension of Fe3O4 MNPs at a known concentration.

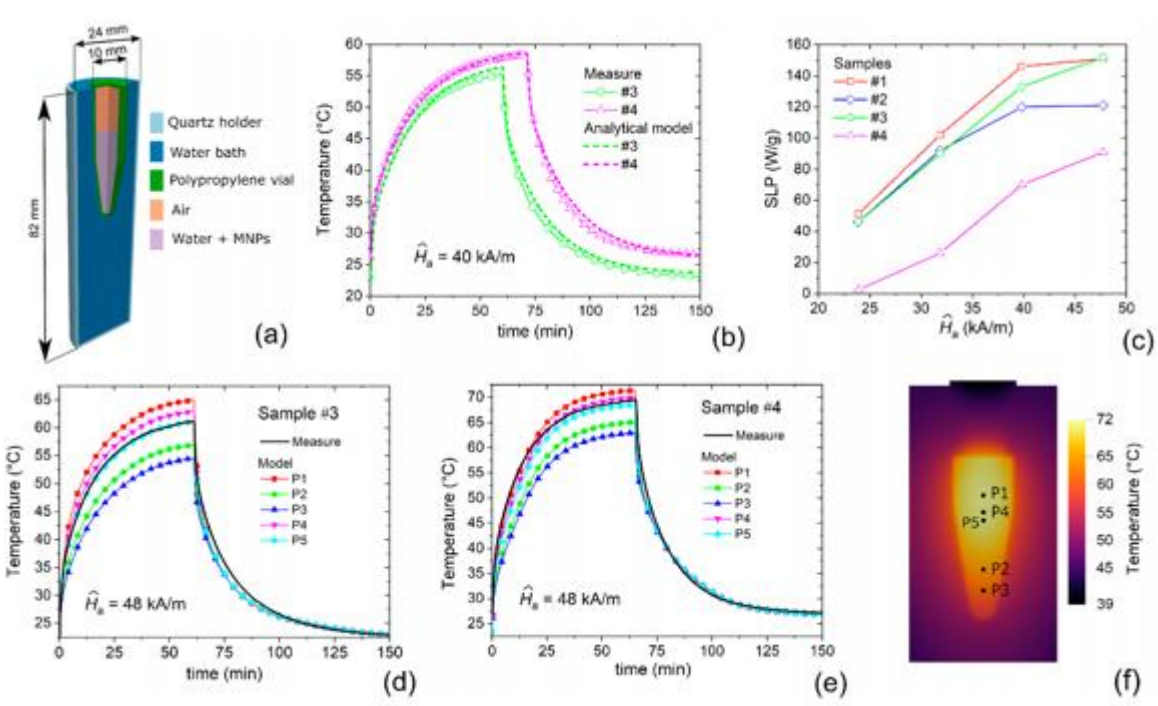

Figure 17 (a) Schematic of the sample container, corresponding to the domain considered for thermal modelling. (b) Time evolution of the temperature of the magnetic solution for samples #3 and #4, fixing the peak amplitude $\hat{H}a$ of the alternating current (AC) magnetic field to 40 kA/m and its frequency to 100 kHz; the graph contains the experimental data and the best fit outputs of the thermodynamic analytical model [45]. (c) Comparison of measured SLP values for all samples as a function of $\hat{H}a$. Comparison between measured and modelled heating-cooling transients for samples (d) #3 and (e) #4, considering $\hat{H}a$ = 48 kA/m. (f) Spatial distribution of the temperature, calculated for sample #4 at the end of the heating interval (t = 65 min), with specification of the points where the temperature time-evolution in (d, e) was evaluated.

Thanks to Researcher Mobility Grant (RMG) contract EURAMET 18HLT06-RMG1 (Development of numerical tools for the simulation of magnetic nanoparticle spatial-temporal distribution in biological tissues) the RMG researcher, in collaboration with VSL, developed a set of numerical tools, based on an open source finite element method library to simulate the transport of magnetic nano particles and their diffusion in cancerous tissues, Figure 18.

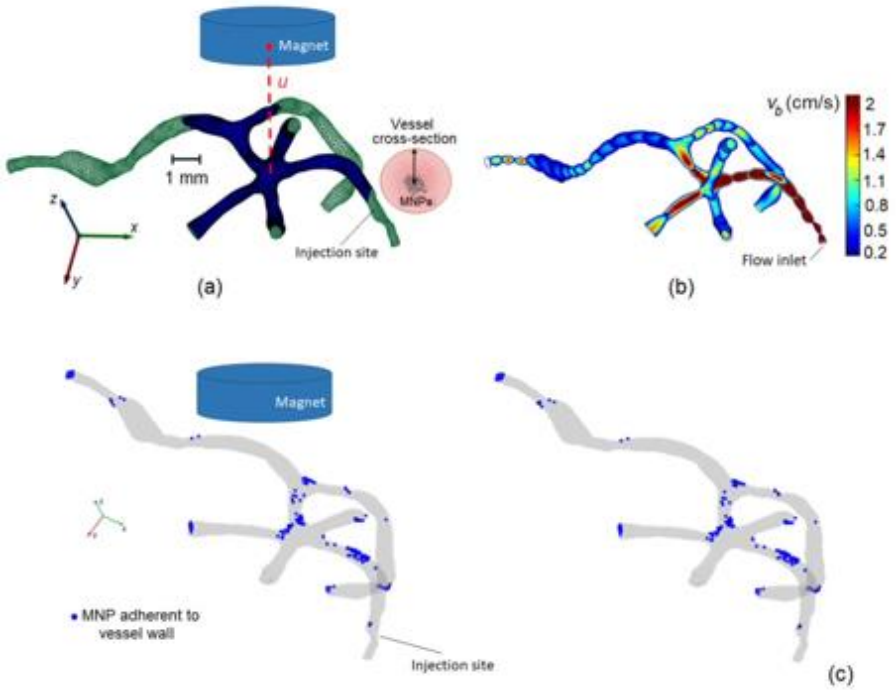

Figure 18 (a) Schematic containing the considered blood vessel segment and the cylindrical magnet, with indication of the MNP injection site. (b) Blood velocity profile within the vessel network. (c) Schematic representing MNPs adhesion along the vessel wall, comparing the results obtained with (left) and without (right) the magnet. The considered magnet has a radius of 1.5 cm, a height of 2 cm and a position defined by u = 1 cm.

The RMG researcher, with support from VSL, researchers developed a series of tools based on the open source FEM computing platform Fenics to evaluate the diffusion of nanoparticle in tissues. The RMG researcher, in collaboration with VSL, ERASMUS MC and TU Delft staff, compared the results of the numerical simulation with nano particles, NPs, diffusion experiments performed in agarose phantom. A set of vials containing agarose gel were injected with a solution of MNPs. A 3D numerical reconstruction of the experiment was performed. The initial diffusion coefficient of the nanoparticle was taken from the available literature. A good agreement was found with the literature, however the agarose phantom showed a much higher resistance to diffusion compared to the tissues, impeding the diffusion of the nanoparticle, Figure 19.

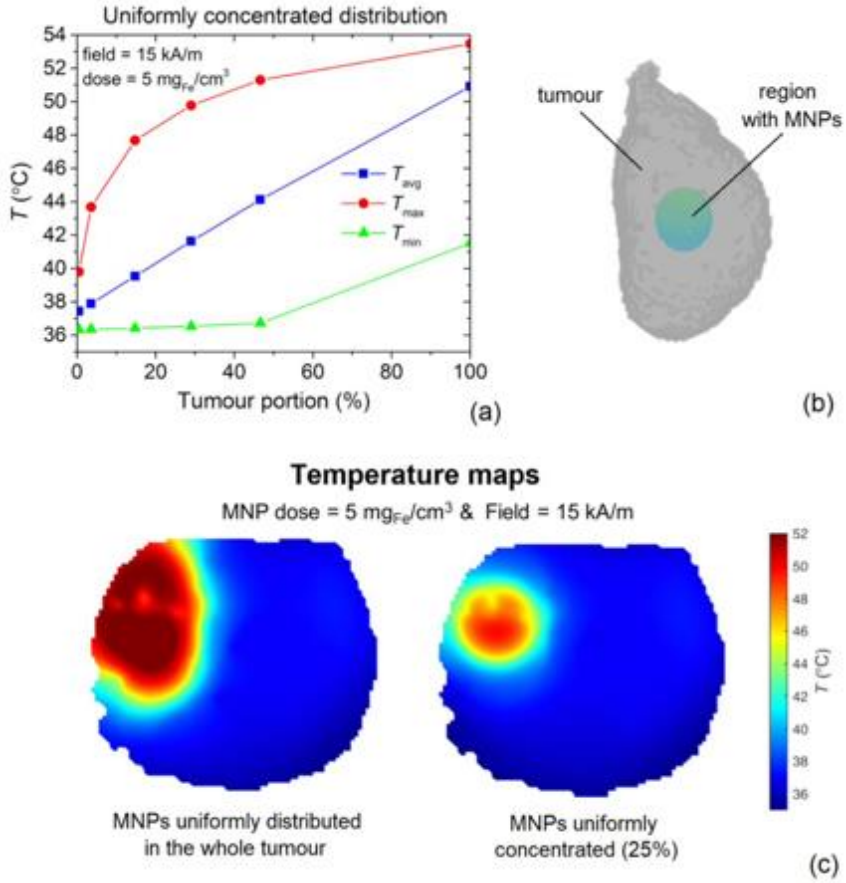

Figure 19 (a) Average, maximum and minimum temperature in the target region, as a function of the tumour portion size where the MNPs are uniformly dispersed (the calculation is performed for a magnetic field of 15 kA/m and a dose of 5 mgFe/cm^3. (b) Schematic of target region (tumour) with the spherical region where MNPs are uniformly dispersed. (c) Maps of the temperature spatial distribution calculated at equilibrium in a body cross section: comparison between the case with MNPs uniformly distributed in the whole tumour (left) and MNPs uniformly concentrated in a tumour portion, corresponding to the 25% of the whole tumour.

One 3D virtual model of a portion of a vascularized cancerous tissue based on a simple ellipsoidal geometry was built by the target volume of the tumour is of 1 cm^3, in accordance with the specification from the project.

Using the numerical code developed two different MNPs infusion strategies (i.e. blood stream injection versus direct injection in the cancerous tissue) were evaluated. Concerning the direct injection strategy a single point and a multipoint injection strategies were compared evaluating the overall homogeneity and concentration of nanoparticle obtained in the tissues, when the same quantity of nanoparticles is administered.

Conclusion:

A finite element numerical tool was developed for the solution of the Maxwell equations in the presence of electromagnetic field sources, to be applied for both magnetic and EMR hyperthermia in the temperature range from 37°C to 50 °C. In parallel, a finite element thermal solver for the bio-heat equation was implemented to determine the temperature increase in tissues, during hyperthermia pre-clinical tests. An ultrasound numerical tool, based on the Westervelt equation, for the simulation of the ultrasound propagation in heterogeneous media like fluids or tissues and the calculation of power deposition was developed. The results were successfully compared with commercial k-wave code.

Methods for the evaluation of temperature resulting from ultrasound exposure using thermocouples were developed. Different models and approaches were considered, for evaluating the effect of positioning, sensor size and sensor artifacts. A method of non-invasive temperature measurement using diagnostic ultrasound was developed that ensures an uncertainty less than 10%. The results were compared with thermocouple methods with good agreement. A thermochromic phantom which changes colour at hyperthermia relevant temperatures was also manufactured and evaluated.

Thermocouples were used to assess the accuracy and repeatability of measurements using MR Thermometry in a commercial device. The results of the comparison have been published on the International Journal of

Hyperthermia.

4.3 To determine by in vitro and in vivo testing, using a metrological approach

Rationale: The purpose of this objective was to determine by in vitro and in vivo testing, using a metrological approach, the efficiency of combined therapies: radiotherapy plus hyperthermia and reverse combination. The spatial-temporal radiation-field characteristics are relevant for the combined radiotherapy/hyperthermia modalities, including radioactive magnetic nanoparticles for simultaneous radiation and heating.

The therapeutic effect of hyperthermia treatment combined with radiotherapy treatment depends on several factors, including the time between treatments, the duration of hyperthermia treatment and the temperature achieved. The combination of the temperature and the duration of heating is known as the thermal dose and is often expressed as the cumulative equivalent minutes at 43°C (CEM43). CEM43 can be used to convert a time-temperature history to an equivalent number of minutes of heating at 43 °C, using the equation:

$$CEM43 = \int t\, R^{(T)} dt \qquad (2)$$

where CEM43 is the cumulative number of equivalent minutes at 43 °C, t is time, T is the temperature and R is related to the temperature dependence of the rate of cell death, $R(T < 43\ °C) = 1/4$, $R(T \geq 43\ °C) = 1/2$

To optimize the efficiency of *in vivo* tests, mainly for ethical reasons, *in vitro* tests were performed to find the best combination HT, mediated by TUS, EMR and MNPs, combined with RT.

4.3.1 in vitro test HT combined with RT

An in vitro test HT (mediated by TUS) combined with RT, was performed by ICR. Using the systems described in 4.1.1 and 4.2.1 (Acoustic Hologram Lenses, AHL) *in vitro* test were performed. Figure 20 shows temperature measurements (a) and the measured acoustic field (b) of the 7-foci lens insonation system.

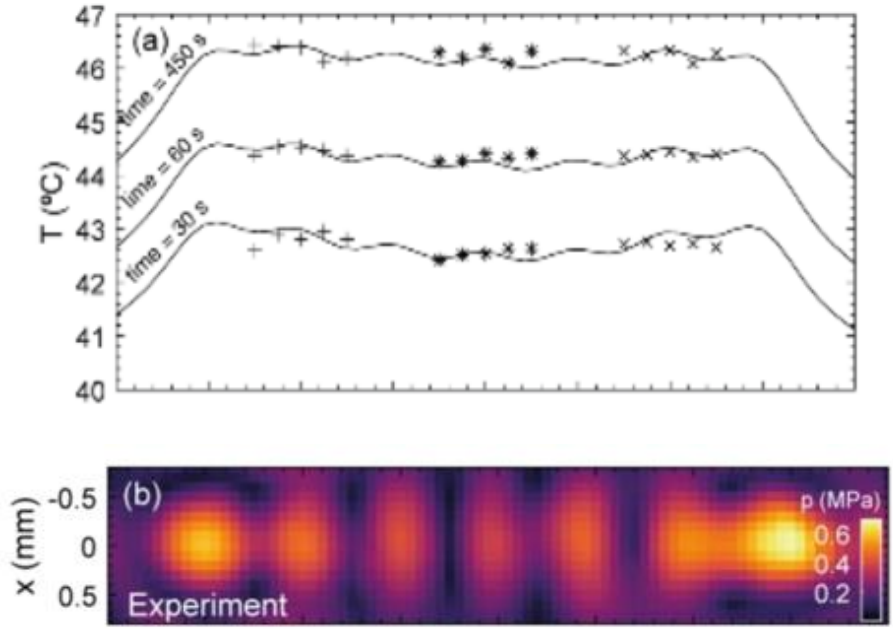

Figure 20 Acoustic a) Temperature profile at different time instants in simulation (solid line) and measured experimentally with each thermocouple, (+) thermocouple 1, (*) thermocouple 2 and (×) thermocouple 3 (b) Measured acoustic field for 7-foci hologram at x-y plane and z = 40 mm (peak pressure).

Spheroid hyperthermia studies were performed by exposing 6 U87-MG tumour spheroids to thermal doses of 7.5, 30, 60 and 120 CEM43. The results demonstrate that viability data suggest a much greater response to treatment than size data. but difficulties with retrieving them from the wells yielded a total of 5 spheroids at 7.5 CEM43, 5 at 30 CEM43, 5 at 60 CEM43 and 3 at 120 CEM43. Eight spheroids were treated as controls. Figure 21 shows the spheroid growth curves. Error bars denote standard deviation between treated spheroids

with each thermal dose. Significant difference values compared to the control are observed when treating spheroids with 30, 60 and 120 CEM43 ($p \leq 0.05$).

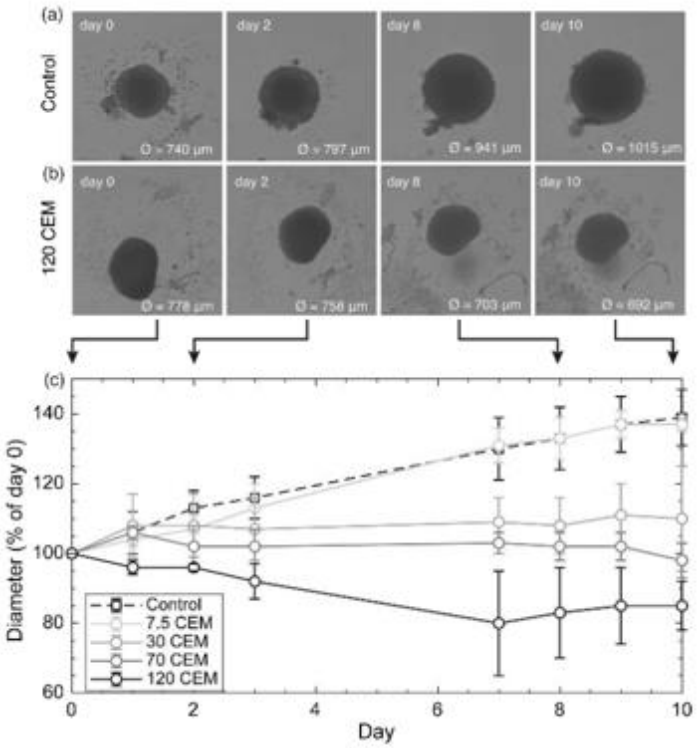

Figure 21 Images of a control spheroids(a) and 120 CEM43 treated spheroid (b) on days 0 (day of treatment), 2, 8 and 10. (c) Growth curves for the control and treated spheroids, as a % of their initial size on day 0. Error bars denote standard deviation in replicate measurements.

Preliminary results show that **the combination of HT (mediated by TUS) combined with RT provides good tumour control over a period of two weeks than RT alone**. In particular these data suggest that the use of HT as a radiosensitizer can reduce the RT dose delivered to the animal and, thus, limit the side effects in normal tissues.

An in vitro test HT (mediated by EMR) combined with RT, was performed by ERASMUS MC and TU Delft in collaboration with INRIM. Using the RF applicator described in 4.1.2 and 4.2.2 in vitro test were performed.

The RF applicator allows well controlled heat delivery and temperature rise within 3D cell cultures (U87 spheroids). In particular, it was designed to guarantee a great reproducibility in terms of power deposition and temperature increase in a target region with a 1 cm^3 volume located at the center of the heating focus. Spheroid cellular activity reduced by:

- 13% at 30 CEM43,
- 26% at 122.3 CEM43,
- 70% at 493.6 CEM43 post HT on day 7, Figure 22.

Microwave-based heat treatment performed at 434 MHz with the RF electromagnetic applicator developed by INRIM and ERASMUS MC showed significant reduction in size as well as cellular activity at higher heat doses, namely, 120 and 480 CEM43. These results were found to be similar to heat doses applied using a water bath.

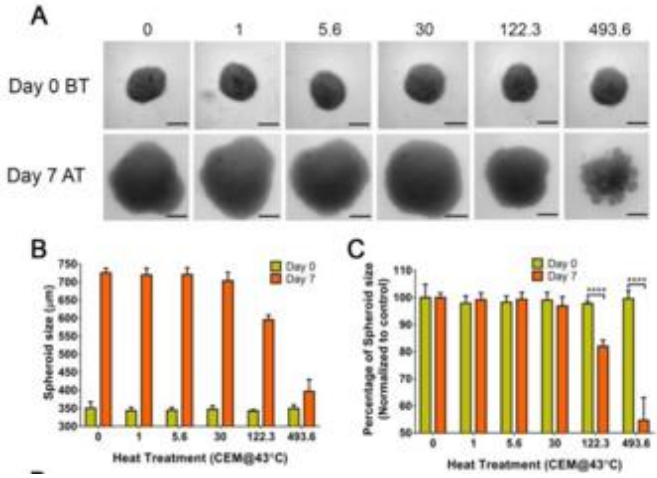

Figure 22 Effect of microwave-based heat treatment on U87 spheroids, performed with the RF applicator. A) Representative spheroid images corresponding to different HT on day 0 and day 7. B) Spheroid size on day 0 and day 7 post heat treatment. C) Percentage of spheroid size normalized to control spheroids on day 0 and day 7 post heat treatment. However, due the limited dimensions of the area where the sample to be irradiated (d = 3.5 cm) is positioned, **the use of the RF applicator developed in preclinical tests is critical**, with the possibility of mouse limb damage or impairment of physiological condition before treatment.

An in vitro test HT (mediated by MNPs) combined with RT, was performed by TU Delft in collaboration with INRIM, TUBITAK, ERASMUS MC and VSL

Using the MNPs described in 4.1.3 and 4.2.3 *in vitro* test were performed. Figure 23 reports the maps of the average, maximum and minimum temperatures evaluated in the target region, as a function of the SLP value and dose. It is interesting to note that, despite the assumption of uniform distribution of the MNPs within the target tissue, the temperature at the end of the heating transient results to be strongly non-uniform, as demonstrated by the large difference between T_{max} and T_{min} found for practically all the combinations of SLP value and dose. This makes the control of temperature during magnetic hyperthermia sessions very critical.

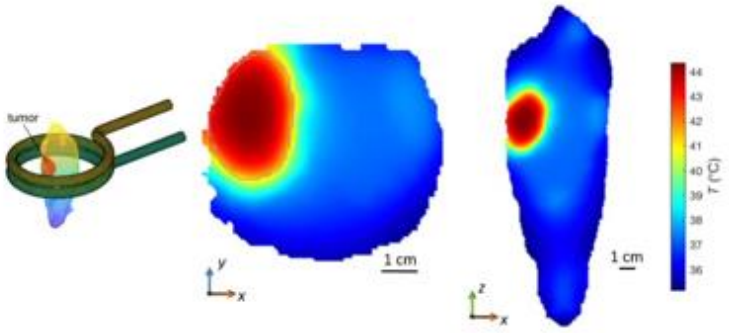

Figure 23 Maps of the spatial distribution of the temperature, evaluated across longitudinal and transverse sections of the rat body when SLP = 100 W/g (found for f = 298 kHz and H_a = 20 kA/m) and the dose of MNPs is 2.5 mg Fe/cm^3.

The *in vitro* experiments suggest that evaluation assays currently available for evaluation of the effects of MNPs heating are not optimal. During incubation, the MNPs completely cover the spheroids and the viability assay implies that a lot of cells are killed at the concentration used, although the size of the spheroid appeared to be much less affected. Lower concentrations however cannot lead to temperatures that are sufficient to affect the spheroids. Additionally, the necessity to wash the spheroids in order to remove MNPs influences the outcome, since this step most probably leads to removal of cells from the surface of the spheroid, which in turn affects its size. These *in vitro* results are also **discouraging for continuation with *in vivo* experiments, using MNPs, at actual stage**, since it was not possible to evaluate what concentration would be needed to see an effect due to heating. At this stage involved partners were also not able to obtain a distribution of the nano-particles to be able to predict the therapeutic effects due to radiation.

4.3.2 in vivo test HT (mediated by TUS) combined with RT

An in vivo test HT (mediated by TUS) combined with RT was performed by OSR in collaboration with INRIM and NPL, using insonation system described in 4.1.1 and 4.2.1 (Far Field Method, FFM).

A glioblastoma (GBM) xenograft nude mouse model obtained by injecting 2x10^6 U87 luc+ cells (glioblastoma cells transfected with luciferase) was used to study the combination of hyperthermia and radiotherapy on the tumour growth. Mice were divided into three groups of six mice each.

The groups received respectively:

(i) **CTRL**, control group, no RT/HT treatments,

(ii) **RT**, RT 6 Gy (RT alone group),

(iii) **RT-HT**, Combination of RT 6 Gy after 1 min HT 42 degree for 8 min.

The HT treatment was delivered 1 minute after RT. The experiment was repeated three times for a total of 54 mice. The ultrasound field was generated by insonation system developed by NPL and INRIM, described in section 4.1.1 and 4.2.1. Radiotherapy was carried out by using a dedicated small animal image guided radiotherapy system (SmART, PXI). The dose planning was based on the CT scan of the animal and performed using the Monte Carlo SmART-ATP treatment planning system. RT has been delivered in a single fraction using 2 opposite beams, Figure 24.

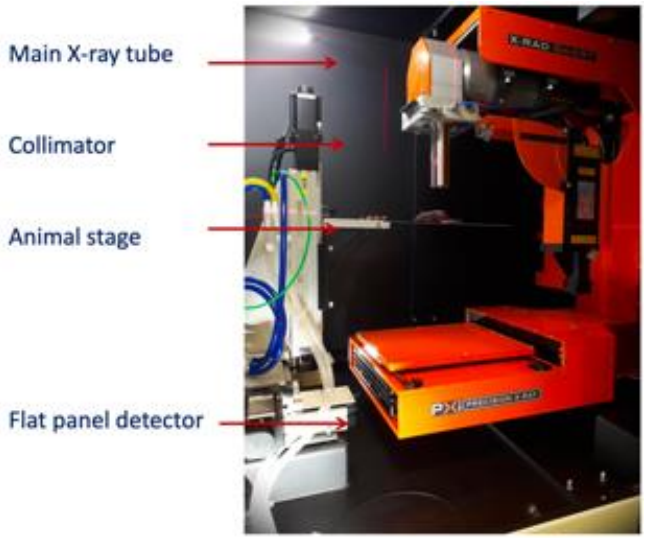

Figure 24 Radiotherapy system (SmART, PXI) used for RT treatments

Two thermocouples were placed between the mechanical cone and the skin mice to measure and control the temperature during the HT treatment, Figure 25.

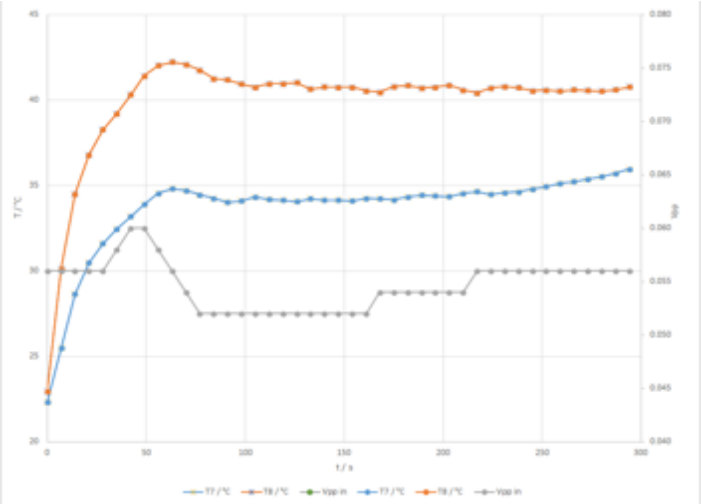

Figure 25 Thermal measurement (red) thermocouple between cone layer and mice skin (blu) thermocouple inside cone layer.

Daily measurements of tumour volume performed with a calliper show a 50% reduction for the HT+RT group with respect to the RT or control groups, Figure 26.

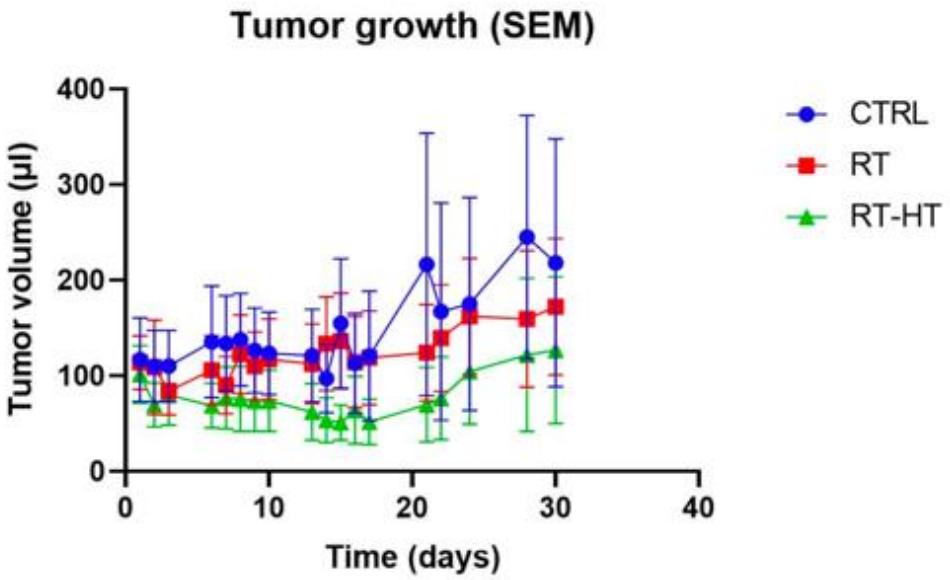

Figure 26 Evolution of the treated tumours *vs* days

An in vivo test HT (mediated by TUS) combined with RT was performed by ICR in collaboration with NPL, using insonation system described in 4.1.1 and 4.2.1 (Acoustic Hologram Lenses, AHL).

Using the same tumour and mouse models as OSR, ICR performed *in vivo* studies using 60 sub cutaneous tumours divided into 4 groups:

(i) **Control** (no treatment),

(ii) **H**, Hyperthermia alone (7.5 or 15 CEM),

(iii) **6Gy**, RT alone (6 Gy),

(iv) **H+6Gy**, Combination of 6 Gy RT and HT for either 7.5 or 15 CEM (RT was delivered approximately 30 minutes after hyperthermia).

Ultrasound hyperthermia was delivered using a bespoke holographically designed lens attached to the 1.5 MHz HIFU transducer of a VIFU wet system (Alpinion Medical Systems Co. Ltd, Republic of Korea), Figure 27 (Left).

The lens split the single geometric focus into 9 foci in a plane 10 mm closer to the transducer. The transducer was driven via a power amplifier (A300 E&I Inc, USA) and function generator (Agilent 33220A). Two 300 micron-diameter K-type thermocouples were placed on the anterior and posterior surface of each tumour in order to measure thermal dose. Radiotherapy was delivered using a dedicated small animal image guided radiotherapy system (SARRP, Xstrahl Ltd, UK) using two opposing beams, in a single fraction, Figure 27 (Right).

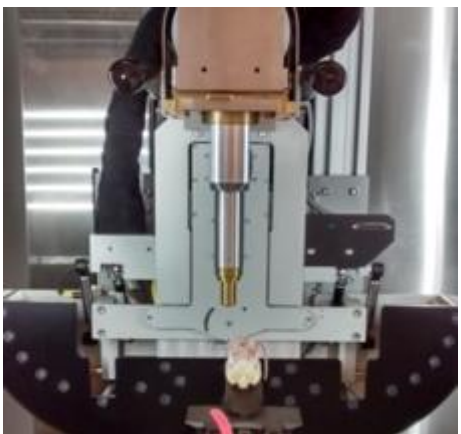

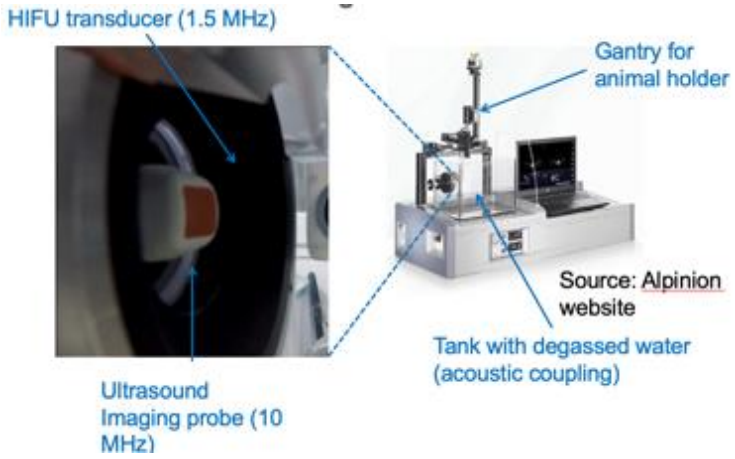

Figure 27 Left, Ultrasound guided TUS system, VIFU, Alpinion, Right Animal radiation platform, SARRP, Xstrahl, Camberley.

The dose planning, based on the cone-beam CT scan of the animal, was performed using the Muriplan software. Caliper measurements of tumour volume, and IVIS luminosity data were obtained every other day. Hyperthermia alone showed faster tumour growth than the control group, but RT and HT+RT showed reduced growth, Figure 28.

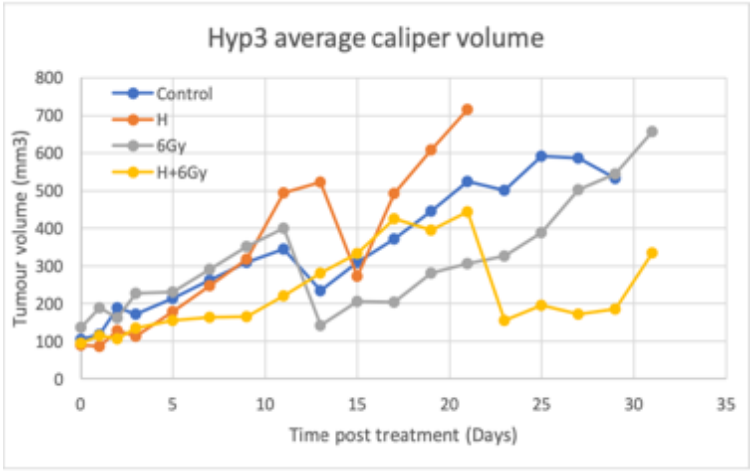

Figure 28 Average measured tumour volume from treatment on Day0 until tumour uncleration when animals were culled.

Conclusion:

A 2.5D and a 3D micromagnetic solver for the solution of the Landau-Lifshitz-Gilbert equation was developed. The codes were applied to calculate the hysteresis losses and the associated specific loss power of nanodisks and nanoparticles, thus providing support to the interpretation of the results from thermometric measurements.

Simulations were performed for various MNPs configurations, i.e., with different shell thicknesses and core diameters. These simulations demonstrate a strong local dose enhancement in the region of 0 – 100 nm around a single MNP which depends on the configuration of the particle.

Three types of magnetic nanomaterials, namely Fe_3O_4 nanoparticles, $Fe_{70}Pd_{30}$ nanodisks and hybrid ^{103}Pd-FeO nanoparticles, were prepared and tested for magnetic hyperthermia application.

A complete set of *in vivo* tests have been performed using RT combined with HT mediated by TUS. A mechanical cone adaptor has been developed to allow use of the HIFU far field. Two thermocouples were placed between the mechanical cone and the skin mice to measure and control the temperature during the HT treatment. Radiotherapy was carried out by using a dedicated small animal image guided radiotherapy system (SmART, PXI). The dose planning was based on the CT scan of the animal and performed using the Monte Carlo treatment planning system.

Acoustic hologram lenses that produce a more uniform thermal dose over complex *in vitro* and *in vivo* biological targets than a single geometric focus HIFU transducer has been developed and tested. The *in vitro* system

was designed for simultaneously treating 3D cells aggregates (spheroids) by using an absorbing phantom with multiple wells each holding a tumour spheroid. Holograms allow a simultaneous targeting providing a uniform thermal dose.

4.4 To develop innovative analytical tools for biological assessment

Rationale: The purpose of this objective was to develop innovative analytical tools for biological assessment by using chemical metrology multimodal techniques as suitable non-invasive and non-ionising tissue diagnosis tools, and mass spectrometry combined with imaging modalities at nanometre resolution.

PTB, NPL and ICR have developed and qualified different analytical methods with respect to their discrimination capability and quantification reliability for biological tissues. Analysis of identical samples by Reference- Free X-Ray Fluorescence analysis, **XRF**, vibrational spectroscopy, Fourier-Transform Infrared Spectroscopy, **FTIR**, and Desorption ElectroSpray Ionisation, Mass Spectrometry Imaging, **(DESI) MSI**, have been performed. These techniques were applied to a small ensemble of different biomedical treated samples, with method described in section 4.3.2, Acoustic Hologram Lenses, AHL, provided by ICR.

XRF measurements for the quantification of trace elements in the different tissue sections were realized at the plane grating monochromator (PGM) for the investigations on light elements (Na, Mg) at the four-crystal-monochromator (FCM) beamline for the investigation of heavier elements such as P, S, Cl, and K. Both beamlines are located in the PTB laboratory at the BESSY II electron storage ring. For each measurement, an ultrahigh-vacuum chamber equipped with a 9-axis manipulator was used as the end station. Within this end station the samples can be precisely positioned and oriented with respect to the incident synchrotron radiation. The X-ray beam spot size on the sample was around 300 µm horizontally and 150 µm vertically at the PGM beamline and around 300 µm horizontally and 180 µm vertically at the FCM beamline.

Absorbance spectra of cryo-sectioned pancreas tissues were recorded in reflection geometry in the MIR spectral range between 3900 cm^{-1} and 900 cm^{-1}. This was done using a Vertex 80v **FTIR** spectrometer (Bruker Optics GmbH) to which a FTIR Hyperion 3000 microscope was coupled both instruments are located in the PTB laboratory at the BESSY. The spectrometer was fitted with a KBr beamsplitter and a globar was implemented as a radiation source for microspectroscopic investigations. For data acquisition, a lN2-cooled multi-element mercury cadmium telluride detector, a so-called focal plane array (FPA) detector with 1282 pixel elements and a spectral resolution of 4 cm^{-1} was used. Micro-spectroscopic experiments on microtome thin tissue sections were conducted with a Cassegrain objective at a 15× magnification, enabling the study of a sample area of 3452 μm^2 at approximately 2.87 µm lateral resolution; the latter corresponds to the dimension of one single pixel.

Desorption electrospray ionisation **(DESI) MSI** was performed using a solvent composition of 95:5 MeOH/H_2O on a Waters Xevo instrument (Waters, UK) in negative ion polarity. The instrument, located in the NPL laboratory, was set to sensitivity mode, and data were acquired using 75 µm pixel sizes in x and y acquired at 2 pixels per second. Data were converted to imzML format using proteowizard and imzML converter, and analyhsed using SpectralAnalysis [49] and in house Matlab scripts (2018b, Mathworks, USA).

Dissected murine syngeneic pancreatic tumours of mice previously treated with low dosages of radiotherapy or hyperthermia as well as sections of healthy mice pancreas were examined, by FTIR and RF XRF or DESI MSI and RF XRF. As DESI MSI is the most time sensitive technique (probing for intact molecules), and destructive towards the surface of the sample, the afterwards investigation of the same samples by FTIR, a surface sensitive technique was not performed. Table 2 shows list of cryo-sectioned pancreatic tissues of mice provided by ICR.

Table 2

Abbreviation	Tissue	Treatment type	Treatment dose	Assessment time	Analysed by
HP	Normal pancreas	N/A	N/A	N/A	RF XRF, FTIR
PC	KPC tumour	RT	N/A	N/A	RF XRF, FTIR
6Gy-D12	KPC tumour	RT	6 Gy	12 d	RF XRF, FTIR
6Gy-D3	KPC tumour	RT	6 Gy	3 d	RF XRF, FTIR
2Gy-D12	KPC tumour	RT	2 Gy	12 d	RF XRF, FTIR
2Gy-D3	KPC tumour	RT	2 Gy	3 d	RF XRF, FTIR
T0	KPC tumour	N/A	N/A	N/A	RF XRF, DESI MSI
T1	KPC tumour	N/A	Luc 2hr	N/A	DESI MSI
T2	KPC tumour	RT	8 Gy	3 hr	RF XRF, DESI MSI
T3	KPC tumour	RT	8 Gy	3 d	RF XRF, DESI MSI
T4	KPC tumour	RT	8 Gy	10 d	DESI MSI
T5	KPC tumour	HT	7.5 CEM	4 hr	DESI MSI
T6	KPC tumour	HT	7.5 CEM	3 d	DESI MSI
T7	KPC tumour	HT+RT	7.5 CEM + 8 Gy	3 d	DESI MSI
T8	KPC tumour	HT+RT	7.5 CEM + 8 Gy	10 d	DESI MSI

The proposed approach is even more effective if the methods are non destructive towards the sample, as the same sample can be investigated. This approach needs samples, which are stable over time. Biological systems can be modified to achieve a certain longevity, for example by various fixation techniques. The drawback is the destruction of most of its original molecular and elemental composition, which are of interest to answer most biomedical questions. The tissues of interest were frozen, sectioned and dyed, to avoid as much chemical preparation as possible, to preserve the original molecular and elemental composition as well as to increase the stability of the sample due to aging.

Thanks to **XRF** measurements, performed by PTB in collaboration with ICR, in the tender X-ray range, large elemental maps for P, S, Cl, and K of G2D3, G2D12, G6D3, G6D12, PC, and HP were obtained. The elemental maps with corresponding violin plots are presented in Figures 29.

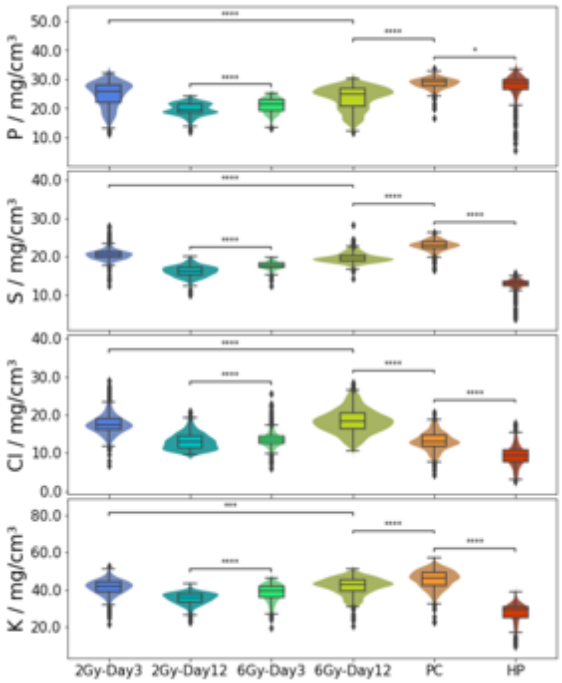

Figure 29 Box plots and violin plots of elemental concentration of P, S, Cl and K showing the occurrence distribution of the concentrations throughout the measured sample area obtained from reference-free **XRF** (analysis of measured tissue samples.

In **FTIR** measurements, performed by PTB in collaboration with ICR, the IR spectral signatures of three pancreas samples are shown in Figure 30 where benign and malign cases are compared, as well as treatment at 6 Gy and fixed 12 days after treatment. Of particular interest is the Amid I band at 1645 cm−1, which will now be analysed in more detail, as the expected changes in protein configuration can induce meaning- full variations in its shape

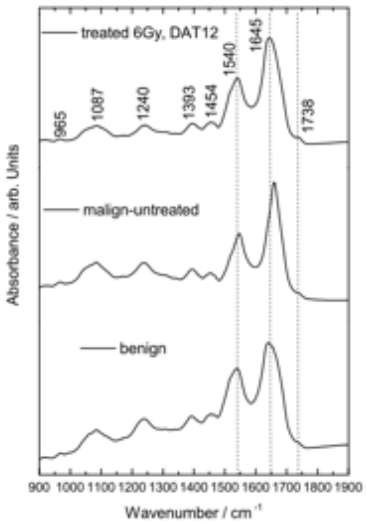

Figure 30 Mid-infrared spectral signatures (arithmetic means of 900 spectra, respectively) of the pancreas samples. The dashed lines display the amide band regions with the most significant spectral changes with respect to band shifts and altered line shapes.

In order to interpret the spectral differences in terms of biomolecular changes in the tissue a ratiometric approach has been developed. To this end the ratios between the secondary structures peak area, grouped according to the different structures, and the area of the entire Amide II peak at 1540 cm^{-1} has been calculated. The result is presented in Figure 31 as blocks of different colour. In addition, the ratio of total area of the amid I band to the amid II band is shown as a blue circle, connected by a line as guide to the eye. The position and area of the FTIR measurement with respect to the sample cross section is shown in the inset for the case of 6Gy- D12. The **FTIR** measurements have been performed on parallel slices as for the XRF measurements above, originating from the same tumour.

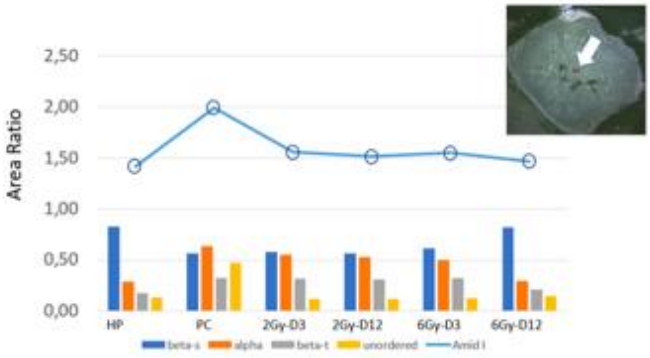

Figure 31 Absorbance ratios of the secondary structure contributions with respect to the amid II band for benign (HP) and malign (PC), as well as treated tissues (2Gy-D3, 2Gy-D12, 6Gy-D3, 6Gy, D12). The position and area of the FTIR measurement with respect to the sample cross section is shown in the inset for the case of 6Gy-D12.

(DESI) MSI measurements, performed by NPL in collaboration with ICR, were made on samples treated with either hyperthermia or radiation, regions with a large reduction in ions tentatively assigned as glutamic and succinic acid, [M-H]-, was observed in the samples 3 days post treatment with hyperthermia, and 10 days post radiation treatment (Figure 32 A and Figure 32 B). In comparison these regions have higher intensities of ions assigned to free fatty acids present such as FA 18:1, and FA 20:4 ([M-H]-) as well as ceramide lipids 32:1 (Figure 32 D and Figure 32 F). These regions could be potentially dead necrotic tissue as indicated by lack of metabolic activity (glutamic acid) and increase in unsaturated fatty acids and ceramides which are pro-apoptotic for pancreatic cancers.

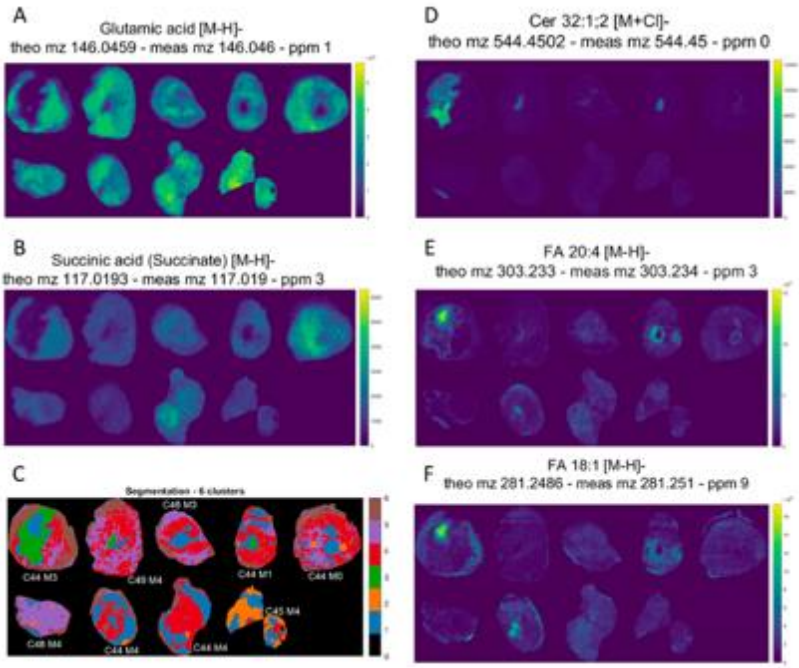

Figure 32 Ions of interest that are either increased or decreased in intensity as a result of radiotherapy or hyperthermia treatment.

In order to better understand the relationship between the elemental and molecular information example tissue image (3 hours post radiation treatment) two sets of images have been registered. This enabled the investigation of the correlation and co-localisation between the elements and molecules in these tissues. Overlay in the distribution of tentatively assigned adenosine monophosphate [M-H]- and sodium in these samples (Figure 33 A), along with an inverse relationship between phosphatidylglycerol (PG) lipid 40:8 [M-H]- and magnesium (Figure 33 B) were observed.

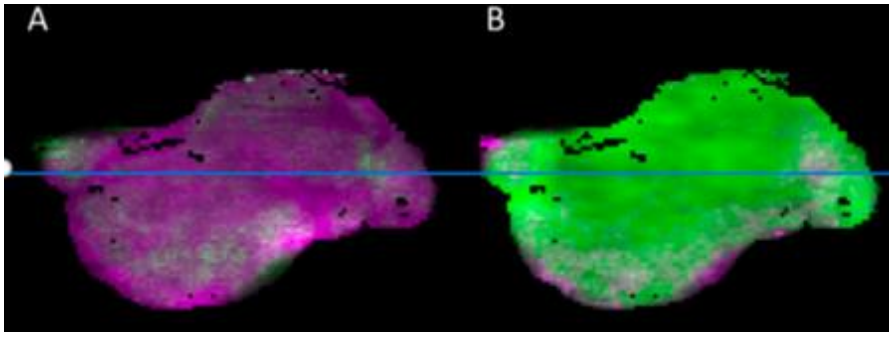

Figure 33 Overlay images of selected ions measured by **MSI** to selected elements measured by **XRF** imaging. A) Overlay of adenosine monophosphate (green) with sodium (magenta) showing similar localisation in the bottom middle of the tissue. B) Overlay of Magnesium (green) with PG lipid 40:8 where the magnesium is present we see a reduction in the intensity of the PG lipid species.

Conclusion:

New systematic metrological approaches using chemical metrology multimodal techniques such as vibrational spectroscopic techniques, FTIR, as suitable non-invasive and non-ionising tissue diagnosis tools regarding chemical species, and SI-traceable X-ray spectrometry for probing elemental compositions, combined with hyperspectral imaging, HIS, modalities at micrometre resolution have been used for biological evaluations. This includes the development of non-destructive metrological strategies and the establishment of reliable measurement procedures (combined with chemometric tools) for the characterisation of biological effects arising from radiotherapy treatments at lateral resolutions on a μm scale. The FTIR-HSI has been widely implemented for detecting and differentiating tumour tissues from benign regions via biomarkers, as well as its potential for tumour grading.

4.5 To facilitate review of the Biological Equivalent Dose (BED) concept

Rationale: The objective was to facilitate the review of Biological Equivalent Dose (BED) concept related to the radiotherapy combined with hyperthermia. The role of control parameters such as the energy deposition in tissues, the radiation dose and the duration of the hyperthermia and/or radiation treatment will be taken into account.

Hyperthermia is a potent sensitizer of cell killing by ionizing radiation (IR). This can be attributed to the fact that heat is a pleiotropic damaging agent, affecting multiple cell components to varying degrees by altering protein structures, thus influencing the DNA damage response. Ionizing radiation induces a variety of DNA lesions, including oxidized base damage, a basic sites, single-strand breaks and double-strand breaks. DNA damage inflicted by ionizing radiation triggers the DNA damage response, molecular events that mostly involve the post-translational modification of proteins that activate intracellular signalling pathways. The activity of the DNA repair processes that deal with such damage has long been known to determine the response to ionizing radiation. Defects in both DNA repair and checkpoint responses in cells affect the response to ionizing radiation and can be exploited for targeted radio-sensitization strategies. Multiple mechanisms contribute to the effectiveness of hyperthermia, with each of these mechanisms requiring a different optimal temperature range. For instance, inhibition of DNA repair is a very effective radiosensitizer, but requires a temperature of at least 41◦C, significantly higher than required for many other mechanisms, such as the reperfusion mechanism which leads to sensitization through reoxygenation, which will occur at more moderate temperatures, starting at 39◦C. There are limited studies investigating the impact of temperature on the radiobiological effects using a systematic variation of the temperature. From these, it is clear that a variation of 1◦C is enough to trigger significant and detectable changes in the radiobiological response as assessed by cell survival and apoptosis. It is therefore recommended that sample temperatures should be estimated with an uncertainty of ±1 oC using a calibrated instrument.

Cell survival curves for specific cell types is one of the methods for evaluation of radiotherapy techniques. For these curves the cell survival (i.e., for a specific biological end-point, often clonogenic survival) is plotted as a function of dose, D. An important aspect in the evaluation is the model used to fit the data. Similarly cell survival curves are used in hyperthermia, where cell survival is plotted as a function of thermal dose (such as CEM43), although the driving mechanism of cell killing is different. In both domains various cell survival models have been proposed or are in use. Evaluation of combined therapies, such as the combination hyperthermia and radiotherapy, requires integration of these models accounting for the driving mechanism of cell killing due to the combined therapy. Thanks to in deep literature review of cell survival models which aim to describe the combination of radiotherapy - hyperthermia has been carried out by ICR, ISS, VSL, NPL, OSR and ERASMUS MC.

The Biological effective Dose (**BED**) offers a quantitative indication of the biological effect induced by any combination of dose per fraction and total dose to a particular tissue characterized by a specific α/β ratio. Its purpose is to compare different fractionation regimes using a common numerical score. It uses a generic α/β ratio = 10 for the early-responding tissues and tumours and α/β ratio = 3 for the late-responding tissues such as normal tissues. The basic BED equation is:

$$BED = n\,d\left[1 + \frac{d}{\alpha/\beta}\right] \tag{3}$$

An initial phenomenological model was based on the attempt to parametrize the alpha and beta dependence on temperature (T) in ºC and temperature exposure time (t) in minutes (i.e. $\alpha(T,t)$ and $\beta(T,t)$. Linear and quadratic dependence for both T and t have been considered resulting in the general model formalism:

$$\alpha(T,t) = \alpha_{37}(1 + k_1(T-37) + k_2(T-37)^2)(1 + k_3 t + k_4 t^2) \tag{4}$$

$$\beta(T,t) = \beta_{37}(1 + q_1(T-37) + q_2(T-37)^2)(1 + q_3 t + q_4 t^2) \tag{5}$$

With α_{37} and β_{37} being the alpha and beta values at 37˚C, while k_1, k_2, k_3, k_4, q_1, q_2, q_3, q_4 are fitting parameters. The model was tested against the available experimental data in order to determine the k and q fitting parameters. Despite the large number of fitting parameters, significant discrepancies were observed between the experimental data and the model prediction (over 200% for some data points). **This seems to indicate that parameterization of the alpha, $\alpha(T,t)$, and beta, $\beta(T,t)$, parameters may not be a suitable approach**.

Despite the complex dependency of the alpha and beta parameters on the Temperature, T, and temperature exposure time, t, a clear trend in the Relative Biological Effect (**RBE**) values for cell survival has been observed. A second phenomenological model was therefore developed and tested based on the observed RBE values. This model was based on the hypothesis that RBE dependence on Temperature and temperature exposure time can be parametrized according to the formalism:

$$RBE = 1 + w(T - 37)t \quad (6)$$

With w being fitting parameters. An independent and linear relationship for both T and t is hypothesized. The w values for different levels of RBE all seems very similar (i.e. independent of the RBE level chosen) with an average of <w> = 0.00508 +/- 0.00017 per T per t.

4.5.1 *Evaluation of RBE using in vitro (RT combined with HT) results*

NPL conducted an extensive set of radiobiological measurements employing the gold standard clonogenic assay and using two different cell lines (MDA-MB-231 cell line, an epithelial, human breast cancer cell line, and MCF7, an epithelial cell line isolated from the breast tissue) with the aim of addressing the role of intrinsic radiosensitivity. The investigations used 6M photons from a Linac with doses ranging from 0 Gy to 5 Gy and temperature treatments of 37°C, 40°C, 43°C and 45°C (preliminary measurements indicated that exposure of cells to 50°C was highly damaging even for a brief period of time) administered by keeping the samples in a water bath for 5 min, 10 min, 15 min or 20 min. All experiments were carried out in triplicate. Data, fitted using the linear quadratic model as:

$$SF = e^{-\alpha D - \beta D^2} \quad (7)$$

clearly indicated an increase radiation effectiveness with both temperature and heating time. The large uncertainties associated with radiobiological measurements, however, prevented the drawing of meaningful conclusions regarding the difference between the two cell lines. Biological effective Dose (BED) and Relative Biological Effectiveness (RBE) were evaluated using the collected data. **Whilst BED was found to be not relevant to the investigations**, RBE assessments at 10% survival increased up to 1.79 for 20 min treatment at 45 °C. Interestingly, the data seem to suggest a plateauing effect with regards to the treatment time (~15 min) with the level of plateau being temperature dependent.

ICR exposed 2D monolayers and 3D spheroids to heat and radiation in vitro. Heat treatments ranged from 37°C (sham exposure) to 47°C applied for up to 15 minutes giving thermal iso-effective doses (TIDs) of 0 to 240 CEM43. The heat was generated using water bath and/or thermal cycler heating (monolayers and spheroids), or HIFU (spheroids only). Radiation doses ranged from 0 to 16 Gy using a CIX2 (X-Strahl) 225 kV cell irradiator. To be able to compare 2D, 3D and in vivo data, a glioma cell line (U87 with or without luciferin construct) was used. Also, breast cancer MCF-7, colon cancer HCT116 and pancreatic cancer KPC/cancer associated fibroblasts mixtures were used as dictated by experimental requirements. Table 4 shows α and β values for the linear quadratic model (7) used to fit the clonogenic data at ICR.

Table 4

Method	Hyperthermia protocol	Dose range	Combination	Cell line	Alpha [Gy-1]	Beta [Gy-2]	Institute
Water bath	37°C, 30 minutes, TID = 0 CEM_{43}	0-6 Gy	Radiotherapy then hyperthermia	U87MG	0.01 ± 0.04	0.005 ± 0.01	ICR
Water bath	43°C, 30 minutes, TID = 30 CEM_{43}	0-6 Gy	Radiotherapy then hyperthermia	U87MG	0.2 ± 0.1	- 0.02 ± 0.01	ICR
Water bath	45°C, 30 minutes, TID = 120 CEM_{43}	0-6 Gy	Radiotherapy then hyperthermia	U87MG	1.43 ± 0.45	- 0.18 ± 0.07	ICR
Water bath	37°C, 30 minutes, TID = 0 CEM_{43}	0-6 Gy	Hyperthermia 24 hours later radiation	U87MG	0.05 ± 0.02	0.002 ± 0.003	ICR
Water bath	43°C, 30 minutes, TID = 30 CEM_{43}	0-6 Gy	Hyperthermia 24 hours later radiation	U87MG	0.28 ± 0.15	- 0.03 ± 0.02	ICR
Water bath	45°C, 30 minutes, TID = 120 CEM_{43}	0-6 Gy	Hyperthermia 24 hours later radiation	U87MG	1.78 ± 0.4	- 0.2 ± 0.04	ICR
Water bath	37°C, 30 minutes, TID = 0 CEM_{43}	0-6 Gy	Hyperthermia then radiation	U87MG	0.01 ± 0.02	0.008 ± 0.004	ICR
Water bath	43°C, 30 minutes, TID = 30 CEM_{43}	0-6 Gy	Hyperthermia 24 hours later radiation	U87MG	0.09 ± 0.11	-0.002 ± 0.01	ICR
Water bath	45°C, 30 minutes, TID = 120 CEM_{43}	0-6 Gy	Hyperthermia then radiation	U87MG	2.16 ± 0.7	- 0.3 ± 0.1	ICR
Water bath	37°C, 30 minutes, TID = 0 CEM_{43}	0-6 Gy	Radiotherapy then hyperthermia	MCF7	0.2 ± 0.04	- 0.02 ± 0.009	ICR
Water bath	43°C, 30 minutes, TID = 30 CEM_{43}	0-6 Gy	Radiotherapy then hyperthermia	MCF7	0.47 ± 0.15	- 0.06 ± 0.02	ICR
Water bath	45°C, 30 minutes, TID = 120 CEM_{43}	0-6 Gy	Radiotherapy then hyperthermia	MCF7	1.42 ± 0.32	- 0.2 ± 0.05	ICR
Water bath	37°C, 30 minutes, TID = 0 CEM_{43}	0-6 Gy	Hyperthermia 24 hours later radiation	MCF7	- 0.02 ± 0.11	0.001 ± 0.02	ICR
Water bath	43°C, 30 minutes, TID = 30 CEM_{43}	0-6 Gy	Hyperthermia 24 hours later radiation	MCF7	0.07 ± 0.1	- 0.01 ± 0.01	ICR
Water bath	45°C, 30 minutes, TID = 120 CEM_{43}	0-6 Gy	Hyperthermia 24 hours later radiation	MCF7	0.2 ± 0.1	- 0.02 ± 0.01	ICR
Water bath	37°C, 30 minutes, TID = 0 CEM_{43}	0-6 Gy	Hyperthermia then radiation	MCF7	- 0.07 ± 0.07	0.02 ± 0.01	ICR
Water bath	43°C, 30 minutes, TID = 30 CEM_{43}	0-6 Gy	Hyperthermia 24 hours later radiation	MCF7	0.09 ± 0.1	- 0.004 ± 0.01	ICR
Water bath	45°C, 30 minutes, TID = 120 CEM_{43}	0-6 Gy	Hyperthermia then radiation	MCF7	0.4 ± 0.06	- 0.04 ± 0.01	ICR

4.5.2 *Evaluation of in vivo (RT combined with HT) tests results*

At OSR, in collaboration with INRIM a glioblastoma (GBM) xenograft nude mouse model obtained by injecting $2x10^6$ U87 luc+ cells was used to study the combination of hyperthermia (HT) and radiotherapy (RT) on tumour growth. For the HT treatments ultrasound field was generated by insonation system described in 4.1.1 and 4.2.1 (Far Field Method, FFM). Radiotherapy was carried out by using a dedicated small animal image guided radiotherapy system (SmART, PXI). The dose planning was based on the CT scan of the animal and performed using the Monte Carlo SmART-ATP treatment planning system. RT was delivered in a single fraction using 2 opposite beams, Figure 34.

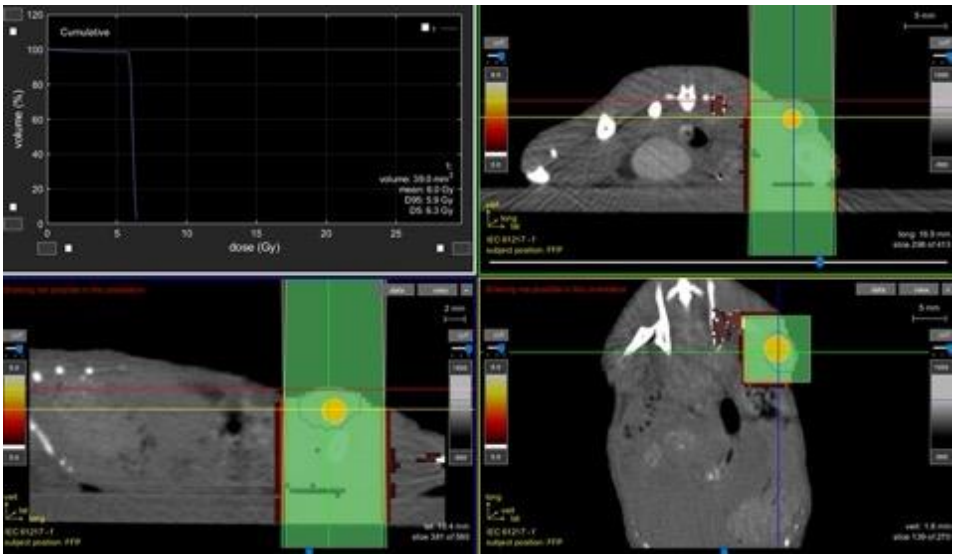

Figure 34 Dose planning based on the CT scan of the animal and performed using the Monte Carlo SmART-ATP treatment planning system.

Daily measurements of tumour volume performed with a calliper show around 40% reduction for the HT+RT group with respect to the RT or control groups. A similar trend has been found using optical BLI, Figure 35.

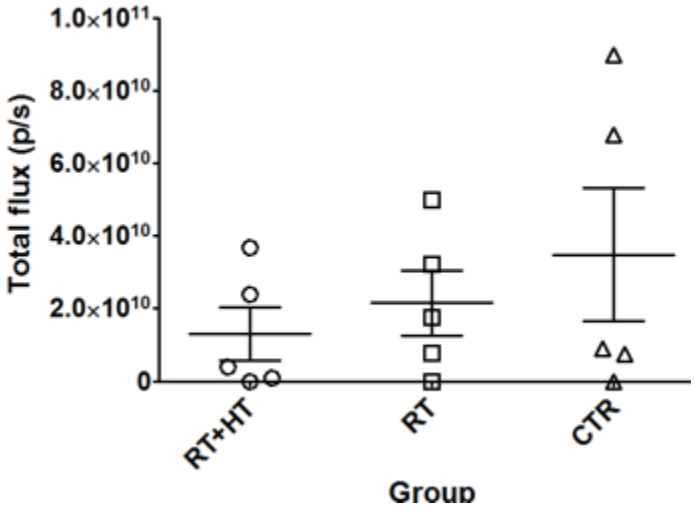

Figure 35 Total flux measured using optical BLI

Conclusion:

An in-depth literature review of the cellular response models (and associated data) used to quantify the synergistic biological effects of combined RT-HT treatments has been performed. This review has been discussed and the alpha-R and LQ models were selected.

The Biological effective Dose (BED) offers a quantitative indication of the biological effect induced by any combination of dose per fraction and total dose to a particular tissue characterized by a specific α/β ratio. Its purpose is to compare different fractionation regimes using a common numerical score. It uses a generic α/β ratio = 10 for the early-responding tissues and tumours and α/β ratio = 3 for the late-responding tissues such as normal tissues.

Different modalities have been employed for the radiation treatment and the hyperthermia. The purpose has been to find which RT-HT protocol would be the most favourable to have a synergistic effect. To quantify the comparison of the different modalities the investigation has mainly used the linear quadratic model in order to obtain a fitting of the parameters α and β.

A glioblastoma (GBM) xenograft nude mouse model obtained by injecting luc+ cells was used to study the combination of hyperthermia (HT) and radiotherapy (RT) on tumour growth. Mice were divided into four groups of six mice each:

1. Control (No treatment)
2. RT alone (6 Gy)
3. HT alone (7.5 or 15 CEM)
4. Combination of 6 Gy RT and HT for either 7.5 or 15 CEM (RT was delivered approximately 30 minutes after hyperthermia).

Daily measurements of tumour volume performed with a calliper show a 50% reduction for the HT+RT group with respect to the RT or control groups. A similar trend has been found using optical BLI, however in this case the differences between the groups is less (15%).

Despite the complex dependency of the alpha and beta parameters on the Temperature (T) and temperature exposure time (t), a clear trend in the Relative Biological Effect (RBE) values for cell survival has been observed. A second phenomenological model was therefore developed and tested based on the observed RBE values. This model was based on the hypothesis that RBE dependence on Temperature (T) and temperature exposure time (t) can be parametrized according to the formalism: RBE = $1+w(T-37)$, with w being fitting parameters. An independent and linear relationship for both T and t is hypothesized.

5 Impact

14 open access articles have been published in peer-reviewed journals. The project has been presented at 52 international and national conferences. One training activity has been carried out regarding the TUS application

in hyperthermia (12 participants from one stakeholder of the project). An e-learning course has been completed and it is available on the RaCHy project website: https://rachy-project.eu/e-learning-course/. The course is titled: Temperature measurements under ultrasound exposure, consisting of four modules: Introduction, Background, Technical Solutions for laboratory measurements and Technical Solutions for clinic measurements. The project website (https://rachy-project.eu) is updated regularly with the latest progress, project updates have also been made available on dedicated pages on Linkedin.

There were more than 50 attendees at the first project stakeholder workshop (VSL, February 2020) '*How the Metrology Can Support Radiotherapy Coupled with Hyperthermia*'. More than 70 attendees (including15 in person), participated at second project stakeholder hybrid workshop (PTB, 23rd November 2021) '*A combined approach for the treatment of tumours*'. Both workshops provided a great opportunity to gather the needs of the stakeholders and share results, or potential results, with the user community. Using input from stakeholders, appropriate tumour lines and biological endpoints for *in vivo* testing of dose reduction were selected during the project stakeholder workshops. A third stakeholder workshop was organized in September 2022 in Sweden, jointly with the annual scientific meeting of the European Society for Hyperthermic Oncology (ESHO). The focus of the workshop was the presentation of the project results, there were around 30 attendees mainly from clinical institutes.

During the Italian celebration of World Metrology Day 2021, the project was presented and discussed to a wide non-technical audience. In addition, three PhD students have presented their studies about HIFU application mechanisms, phantom production, ultrasonic power measurements and temperature investigations in phantoms to researchers.

As an alternative to the 2021 European Researchers' Night at the Istituto Superiore di Sanità (ISS), which was suspended due to Covid-19, the consortium gave an informal presentation of the project at the entrance of the ISS (PlanISSfero, which stands for ISS research planisphere).

Two Special Session have been organised: "Materials characterisation, SPM techniques and European project highlights" within E-MRS ALTECH 2021 - Analytical techniques for precise characterization of nano materials and "Hyperthermia techniques - Update from the EMPIR RaCHy Project" within Mathematical and Statistical Methods for Metrology (MSMM 2021).

The project results have been presented during the EURAMET TC-AUV and TC-IR annual meetings. Thanks to a strong collaboration with IEC TC 87 Ultrasonics, project outcomes have been shared with the members of the technical committee. During the 13th BIPM Consultative Committee for Acoustics, Ultrasound and Vibration (CCAUV) virtual meeting the project progress was presented by the TC-AUV Chair to the CCAUV delegates and experts.

Impact on industrial and other user communities

The first group of beneficiaries will be the cancer research community, who will be provided with metrological instruments that are able to perform reliable, repeatable and transferrable tests of nanoparticles and ultrasound-based methods for quantitative determination of temperature profiles. The next group of beneficiaries is the medical device industry, who will be provided with the knowledge and tools required to develop new medical equipment, such as a laboratory US insonation system. Another group of beneficiaries are the hospitals who will be provided with calibration devices to help measure the performance of the new equipment and a metrological framework for clinical trials to ensure the uniformity of trials and the application of trial-results of test temperature accuracy and reproducibility of TUS heating.

The regulation industries that are involved with Quality Assurance for HIFU devices and safety assessment for diagnostic devices will immediately obtain an advantage from the evaluation of temperature profiles during ultrasound exposure carried out in this project. Accurate measurement of the output of HIFU machines will reduce the maintenance costs of the equipment, allow defects to be detected quickly and prompt interventions to be made, thus reducing shutdown times.

FDA U.S. Food & Drug Administration, Istituto Neurologico Carlo Besta, FUS, Focused Ultrasound Foundation ESHO, European Society for Hyperthermic Oncology and stakeholders have demonstrated an interest in the development of techniques and methods for hyperthermia mediated by ultrasound. They provide interesting opportunities for exploitation of the project results. The solution based on acoustic holograms can be helpful on getting uniform thermal doses for large volume in vivo tumours, when constant temperature over a wide area is needed. In this case, patient-and-target-specific holograms should be designed, because the acoustic field should be tuned to compensate the balance between heating rate and heat transport along the therapeutic acoustic image. Project results demonstrate that tunned holographic lenses coupled to single-element transducers can be applied to obtain uniform thermal doses over wide areas or complex targets, using a low-cost but robust system. Further work can be done to optimize thermal uniformity in complex 3D targets, for example, applying optimization and machine learning algorithms to tune the holograms for uniform thermal

dose. Other strategies for a deep control of the acoustic field include broadband phase-and-amplitude holograms, locally resonating metamaterials, or spatial sound modulators, to engineer the acoustic wavefront and produce uniform thermal patterns for ultrasound hyperthermia systems.

Impact on the metrology and scientific communities

The interaction with metrological and standardisation bodies is ongoing, and is implemented through the involvement of consortium partners in EURAMET technical committees (TC-AUV, Technical Committee for Acoustics, Ultrasound And Vibration, TCAUV SC-U, TC-AUV subcommittee Ultrasound and Underwater Acoustics, TC-IR, Technical Committee for Ionising Radiation, 19NET04 MIRA, Support for a European Metrology Network on the medical use of ionising radiation) and in national and international standardisation bodies (CEI TC29/87 Electroacoustics/Ultrasound, CEI SC 62C -Equipment for radiotherapy, nuclear medicine and radiation dosimetry-, IEC TC87 -Ultrasonics-, U.S. FDA, Food and Drug Administration).

Instruments and methods have been developed within the project, that will be useful both at a metrological research level and in clinical settings. The main ones are (i) a new RF applicator based on a coaxial TEM system, able to generate a uniform power deposition pattern at a frequency of 434 MHz, and suitable for the calibration of EMR hyperthermia setups; (ii) an ultrasound system based on HIFU transducers using the far field properties, that makes possible the treatment (by hyperthermia) of cancer tissues up to 10 mm diameter, guaranteeing the control of power deposition and temperature increase during treatments. Ultrasound and Electromagnetic field exposure assessment and the development of well calibrated applicators will be beneficial for the metrology community and for preclinical studies.

Hyperthermia is the process of raising tissue temperatures in the range 40°C - 45°C for a prolonged time (up to hours). The ability to maintain a certain temperature in a target region is key to a hyperthermia delivery system.

The research activities and the comparison of different measurement methods are expected to benefit the US Technical Standard Committee working groups. Material and phantoms developed and tested in the project were designed with the following criteria: to simulate biological tissue acoustically and thermally, to provide real-time feedback of the temperature, and to include a thermochromic material to provide both an indicator of exposure area and the temperature reached in a biologically relevant environment. A report has been sent to IEC TC 87-Ultrasonics- chair to evaluate the application on technical specifications.

The EMR scientific community is also expected to benefit from the use of novel heat mediators prepared via advanced nanotechnology fabrication processes. An accurate characterisation of their magnetic properties, combined with micromagnetic modelling, could also provide indications for their alternative use as new contrast agents in Magnetic Resonance Imaging, MRI, or tracers in Magnetic Particle Imaging, MPI.

Relevant scientific results, related to MNP design field, are expected from the investigation of dual functional MNPs, made of a magnetic shell and a radioactive core, considering the complexity of evaluating their efficacy, due to the simultaneous delivery of heat and radiation. Understanding their behaviour could also have an impact on the design of novel Positron Emission Tomography, PET, or MRI contrast agents.

In general, a rigorous assessment of different techniques, with the relevant uncertainties, could be exploited in different US and EM medical application fields, over and above those envisaged in this project, for example, diagnostics (US or Magnetic Resonance, MR, imaging and the related dosimetry aspects), high intensity ultrasound therapy and thermo-ablation treatments. In this framework, a strong support can be also provided by *in silico* models, able to guide the development of the hyperthermia applicators towards a more controlled heat release and temperature rise.

Impact on the relevant standards

The impact within the clinical community is strengthened by the involvement of EU oncology research institutions in the consortium. These partners and some stakeholder committee members are also active members of relevant scientific associations including ESHO, European Society of Hyperthermic Oncology and ESTRO, European Society for Radiotherapy and Oncology. Thanks to these links, the consortium was able to identify the best research strategy and, at the same time, maximize impact to the end user (in this case the oncology research centres and hospitals).

In particular the consortium has close links with IEC TC 87 – Ultrasonics. A report on the results of a comparison between different techniques for the measurement of temperature based on thermochromic phantoms and ultrasound-based techniques was prepared. The report was sent to IEC TC 87 chair to evaluate the application on technical specifications, TS-63081: *Methods for the characterisation of the ultrasonic properties of materials* and TS-62900: *Measurement- based simulation in water and complex media*.

ISO/TC 229 has accepted the proposal for a standard for magnetic beads for DNA extraction formally as a new project in the committee's work programme. Static hysteresis loops have been measured following the

protocol indicated in the first standardization documents on Magnetic NP, ISO/TS 19807-1 “Magnetic nanosuspensions”. However, this document contains the basic terms for characterisation of magnetic nanomaterial and lists measurement methods, without giving any detailed prescription on how to perform measurements.

There are two standards (ISO 22761 and ISO 19807-2) that are mainly focused on measurements in Fe_3O_4 oxides nanoparticles. By measuring SLP, and more generally magnetic properties also of other types of MNPs, like FePd nanodisks, using the standards implemented/assessed in the EMPIR 16NRM04 MagNastand project, RaCHy project will broaden scientific knowledge to pave the way for the exploitation of MNPs in biomedicine.

Longer-term economic, social and environmental impacts

It has been estimated that the total cost of cancer treatment and management in Europe is €126 billion/year, with the majority being used for healthcare expenses, including doctors' time and medicinal costs. The loss of productivity, due to sick days or people dying young, costs €52 billion/year, while the cost of providing care for bereaved families is estimated to be about €23 billion/year. The European external beam radiotherapy device market, which is mainly driven by the rapidly changing cancer treatment technology and the growing number of cancer patients, is expected to exceed €650 million by 2020.

Longer term, the clinical availability of the techniques developed in this project will be of benefit to patients and society as a whole as Europe faces greater pressures from the increased number of patients that have to be treated as a result of a growing and ageing population. Survival rates and quality of life will improve, as it will be possible to reduce the radiation dose for patients without affecting the therapeutic outcomes, and this will result in reduced toxicity, which in turn will improve the patients’ quality of life as well as reduce the burden of care. It will also be possible to reduce the dose, and as a result a greater number of patients will be admissible for treatment. On the other hand, it will be possible to deliver an increased effective dose with the same toxicity in order to target radio-resistant regions, such as hypoxic regions, thus improving the efficacy of treatments.

6 List of publications

[1]. G. Durando, P. Miloro, V. Wilkens, B. Karaboce, J.De Pooter, G. Van Rhoon, G. Ter Haar, B. Caccia, A. Spinelli, A. Denkowa, R. Dijkema, EURAMET EMPIR 18HLT06 RaCHy Project: Radiotherapy coupled with Hyperthermia (Induced by HITU), Proceedings of the 23rd International Congress on Acoustics, DOI: https://doi.org/10.18154/RWTH-CONV-238838

[2]. M. Marschall, A. Hornemann, G.Wubbeler, A.e Hoehl,1 E.Ruhl, B. Kastner, C. Elster1, Compressed FTIR spectroscopy using low-rank matrix reconstruction, Optics Express, Vol. 28, Issue 26, pp. 38762-38772 (2020), DOI: https://doi.org/10.1364/OE.404959

[3]. G. Ulrich, E. Pfitzner, A. Hoehl, J.-W. Liao, O. Zadvorna, G. Schweicher, H. Sirringhaus, J. Heberle, B. Kastner, J. Wunderlich, D. Venkateshvaran, Thermoelectric nanospectroscopy for the imaging of molecular fingerprints, Nanophotonics, Volume 9: Issue 14, DOI: https://doi.org/10.1515/nanoph-2020-0316

[4]. Minutoli, D., CACCIA, B., Campa, A., Durando, G., Pozzi, S. and Valentini, S. How to make FAIR a project: open access to research data and the RaCHy - Radiotherapy Coupled with Hyperthermia, Notiziario dell’ISS, Volume 34, Issue 1, DOI: https://doi.org/10.5281/zenodo.5728941

[5]. A.Manzin, R. Ferrero, M. Vicentini, From Micromagnetic to In Silico Modeling of Magnetic Nanodisks for Hyperthermia Applications, Advanced Theory and Simulations, Volume 4, Issue 3, DOI: https://doi.org/10.1002/adts.202100013

[6]. Ferrero, R., Barrera, G., Celegato, F., Vicentini, M., Hüseyin, H., Yıldız, N., Atila Dinçer, C., Coïsson, M., Manzin, A. and Tiberto, P. Experimental and Modelling Analysis of the Hyperthermia Properties of Iron Oxide Nanocubes, Nanomaterials, Volume 11, Issue 9, DOI: https://doi.org/10.3390/nano11092179

[7]. F. Foglietta, G. Gola, E. Biasibetti, M.T. Capucchio, I. Bruni, A. Francovich, G. Durando, E. Terreno, L. Serpe, R. Canaparo, 5-aminolevulinic acid triggered by ultrasound halts tumor proliferation in a syngeneic model of breast cancer, Pharmaceuticals, Volume 14, Issue 10, DOI: https://doi.org/10.3390/ph14100972

[8]. F. Foglietta, V. Pinelli, F. Giuntini, N. Barbero, P. Panzanelli, G. Durando, E. Terreno, L. Serpe, R. Canaparo, Sonodynamic treatment induces selective killing of cancer cells in an in vitro co-culture model cancers, Volume 13, Issue 15, DOI: https://doi.org/10.3390/cancers13153852

[9]. P. Miloro, S. Ambrogio, F. Bosio, R.M. Baêsso, B. Zeqiri, F. Fedele, and K.V. Ramnarine, A standard test phantom for the performance assessment of magnetic resonance guided high intensity focused ultrasound (MRgHIFU) thermal therapy devices, International Journal of Hyperthermia, Volume 39, Issue 1, DOI: https://doi.org/10.1080/02656736.2021.2017023

[10]. A.Manzin, M.Vassallo, R. Ferrero, M. Vicentini, In silico experiments as a tool to reduce preclinical tests of magnetic hyperthermia, Proceedings of Third Centro 3R Annual Meeting (Biomedical Science and Engineering), Volume 4, Issues s1, DOI: https://doi.org/10.4081/bse.2021.199

[11]. Librizzi, L., Uva, L., Raspagliesi, L., Gionso, M., Regondi, M.C., Durando, G., DiMeco, F., de Curtis, M. and Prada, F. Ultrasounds induce blood–brain barrier opening across a sonolucent polyolefin plate in an in vitro isolated brain preparation, Scientific Reports, Volume 12, Issues 1, https://doi.org/10.1038/s41598-022-06791-7

[12]. Manzin A., Ferrero R., Androulakis I., Martino L., Nadar R., van Rhoon G.C. Design and characterization of an rf applicator for in vitro tests of electromagnetic hyperthermia, Sensors, Volume 22, Issues 10, DOI: https://www.mdpi.com/1424-8220/22/10/3610

[13]. A. M Ivory, R. de Melo Baesso , G. Durando , S. Rajagopal , P. Miloro Development and testing of a system for controlled ultrasound hyperthermia treatment with a phantom device, Transactions on Ultrasonics, Ferroelectrics, and Frequency Control, DOI: https://ieeexplore.ieee.org/document/10012378

[14]. M. Vassallo*, D. Martella, G. Barrera, F. Celegato, Marco Coïsson, R. Ferrero, E. S. Olivetti, A. Troia, H. Sözeri, C. Parmeggiani, D. S. Wiersma, P. Tiberto, A. Manzin Improvement of Hyperthermia Properties of Iron Oxide Nanoparticles by Surface Coating, ACS Omega DOI: https://doi.org/10.1021/acsomega.2c06244

This list is also available here: https://www.euramet.org/repository/research-publications-repository-link/

7 Contact details

Coordinator: Giovanni Durando, INRIM

Tel: +39 011 3919 353

E-mail: g.durando@inrim.it

Project website address: www.rachy-project.eu